Clemson University
TigerPrints

All Theses | Theses

5-2011

INTEGRATING PHASE CHANGE MATERIALS IN BUILDING MATERIALS: EXPERIMENTATION, CHARACTERIZATION AND NUMERICAL SIMULATION

Esvar Subramanian
Clemson University, vblouin@clemson.edu

Follow this and additional works at: https://tigerprints.clemson.edu/all_theses

 Part of the Materials Science and Engineering Commons

Recommended Citation
Subramanian, Esvar, "INTEGRATING PHASE CHANGE MATERIALS IN BUILDING MATERIALS: EXPERIMENTATION, CHARACTERIZATION AND NUMERICAL SIMULATION" (2011). *All Theses*. 1073.
https://tigerprints.clemson.edu/all_theses/1073

This Thesis is brought to you for free and open access by the Theses at TigerPrints. It has been accepted for inclusion in All Theses by an authorized administrator of TigerPrints. For more information, please contact kokeefe@clemson.edu.

INTEGRATING PHASE CHANGE MATERIALS IN BUILDING MATERIALS: EXPERIMENTATION, CHARACTERIZATION AND NUMERICAL SIMULATION

A Thesis
Presented to
the Graduate School of
Clemson University

In Partial Fulfillment
of the Requirements for the Degree
Master of Science
Materials Science and Engineering

---

by
Esvar Subramanian
May 2011

Accepted by:
Dr. Vincent Y. Blouin, Committee Chair
Dr. Erik Skaar
Dr. Kathleen A. Richardson

ABSTRACT

Phase Change Materials (PCM) have many commercial applications, including in buildings to reduce cooling and heating loads. However, the lack of research has prevented their use as a common building material. This research is part of a larger project that aims at developing a set of practical design guidelines for integrating PCM in buildings. A review of and classification of common PCM available on the market is provided. The thesis then focuses on the experimental characterization of the thermo-physical properties of PCM-integrated building materials and the development of a numerical model for the thermal analysis of buildings with PCM. Different types of PCM are mixed in plaster, a building material used for wall surface finish. The main thermal properties of interest are the thermal conductivity, latent heat, and melting and solidification temperatures. Differential scanning calorimetry is conducted to determine the phase change temperature and the latent heat. A thermopile is used to measure thermal conductivity. A Finite Element numerical model of a wall assembly is used to conduct parametric studies and predict building energy consumption.

DEDICATION

I dedicate this thesis to my parents Mr. S.Ganapathy Subramanian and Mrs. R.Meenakshi and also to my aunt Ms. R.Sethumadhavi

ACKNOWLEDGMENTS

I would like to thank my advisor, Dr. Vincent Blouin, for his continuous support, encouragement and patience.

Additionally, I would like to acknowledge my colleagues Mr. Dominic Triana and Ms. America Murray for their intellectual support and assistance in carrying out some of the experimental work. I would also like to specially thank Dr. Kathleen Richardson who helped me in testing times. I would also like to thank Dr. Eric Skaar for his constant encouragement.

TABLE OF CONTENTS

Page

LIST OF TABLES

LIST OF FIGURES

List of figures (Continued)

Figure Page

CHAPTER 1

INTRODUCTION

1.1 Background

The building industry, an ever-growing field, is considered one of the largest consumers of energy. Approximately, it consumes 40% of the available global energy. In addition, overall economic development has led to a rise in the standard of living and, hence, an increase in the use of air conditioners, heating and cooling devices, further increasing the energy consumption of the building industry in addition to contributing to climate change. The heating, ventilation and air conditioning systems (HVAC) in such buildings must provide both thermal comfort and acceptable ventilation for occupants without sacrificing energy efficiency [1].

Thus, the design of buildings and the optimization of the HVAC systems should be achieved to increase energy efficiency in the construction of modern buildings. The depletion of reserves of fossil fuels (not renewable) and the legislation of environmental protection necessitate the use of thermal energy storage systems. The development of such systems received much attention from builders, architects and engineers during the last decade. Also, the primary advantage of their energy efficiency during on peak load conditions has made it possible for bringing down the building energy cost [1].

The widening gap between global demand and supply of energy is so challenging for the engineering community that great emphasis is laid on energy efficiency and hence

experts turn towards the utilization of naturally available alternate energy sources like solar, wind and hydroelectric. As far as the building industry is concerned direct solar radiation is one of the most promising sources of energy in many parts of the globe even though it is of intermittent nature. Hence an effective technology needs to be developed for large scale storage and use of solar energy in buildings.

Thermal energy storage systems can be sensible heat storage systems, latent heat storage systems or a combination of both [2]. In the former the temperature of the storage material changes as the energy is stored and retrieved, while latent heat storage makes use of the energy stored when a substance changes from one phase to another by melting or solidification. During this phase change the temperature of the material remains the same. Thus, the materials used in latent heat thermal storage (LHTS) units undergo change of phase (solid to liquid) and vice versa during the energy transfer process. Phase Change Materials (PCM) are used for the purpose of storing thermal energy by means of the large latent heat of such materials when changing phase usually between the solid and the liquid state. A phase change involves a large amount of latent energy at small temperature changes Therefore PCMs are used for temperature stabilization and for storing heat with large densities in combination with rather small temperature changes.

The heat storage capacity of the material depends on both its specific heat and latent heat values. Thus, it is preferable for the storage material to have high specific heat capacity and latent heat values [3]. Phase change materials were first used in British transport to prevent trains from becoming too cold in the winter [4]. The application of

PCMs for heating and cooling purposes in buildings was investigated and published in 1975 in the report by Telkes [5]. In 1980, Bordeau tested a passive solar collector containing $CaCl_2 .6H_2 O$ finding that a 8.1-cm thick PCM wall had an appreciable thermal accumulation [6]. In 1986, Lane reported that by impregnating the porous construction materials such as plaster with PCMs can significantly increase the thermal mass and enhance the possibility of heating and cooling buildings [4].

The idea of using PCMs for cooling has also been tested and applied in the case of air conditioners. At night the PCM is cooled due to ambient conditions releasing the cold into the inner regions of the building during the warmer daytimes. This concept is known as free cooling [7-10].

PCMs have a wide variety of uses in buildings including integrated space heating, integrated cooling systems, and integrated combined heating and cooling systems. They are also used in air conditioning, in thermally activated ceiling panels and in incorporation in building materials [11].

PCMs should have a high energy storage density for their successful use. Also, they should be able to charge and discharge the stored energy with a thermal power adapted to the desired application. The transient heat transfer is governed by heat storage and also heat conduction. Being able to store heat assumes that the heat can be transported by means of conduction to the PCM. The capacity in storing the heat at the proper rate depends on conductivity. Thus, we need to know exactly the conductivity of all materials involved in the heat transfer process. In addition, one major drawback of

latent heat storage systems is the low thermal conductivity of materials used as PCM or the materials that encapsulate the PCM, which restricts the energy that can be stored and released from it [11].

1.2 Research Objectives

The lack of research has prevented the use of phase change materials as a common building material. The research presented in this thesis is part of a larger project that aims at developing a set of practical design guidelines for integrating PCM in buildings. This thesis focuses on the experimental characterization of the thermo-physical properties of PCM-integrated building materials and the development of a numerical model for the thermal analysis of PCM-integrated building wall systems. PCMs are usually used by incorporation into a pre-existing material such as plaster, gypsum and concrete. The research goals can be listed as follows:

- Conduct a review of existing PCMs available on the market for building applications.

- Use differential scanning calorimetry to determine the phase change temperature and the latent heat of samples consisting of PCM within a plaster matrix.

- Develop an experimental thermopile to measure the thermal conductivity of the same samples and determine the effect of the presence of PCM on thermal conductivity.

- Develop a Finite Element numerical model of a wall assembly for conducting parametric studies in terms of conductivity and location of PCM and study their effect on energy consumption.

1.3 Thesis Outline

The first chapter includes the introduction with the background on phase change materials and the research objectives. The second chapter presents a detailed review of the literature aiming at describing the properties of phase change materials and classifying them. The third chapter covers the experimental techniques for measuring the phase change temperature and the corresponding latent heat. The fourth chapter deals with experimental measurement of thermal conductivity. The fifth chapter deals with the numerical modeling. The sixth chapter concludes the thesis and presents future work.

CHAPTER 2

PHASE CHANGE MATERIALS

After World War II, research began on solar heat storage, with researchers focusing on the investigation of latent heat systems (LHS) [2]. Salt hydrates, which were readily available and relatively inexpensive, generated much interest in LHS. However, due to the variations in their thermal behavior and progressive drifting of the transition zone over repeated phase change cycles, further research found them to be unreliable [2]. As a result, anhydrous organic substances (poly-ethylene glycol, fatty acids and their derivatives, and paraffins) became preferred, despite their higher cost and low heat storage capacity per unit volume [2,3]. Nowadays, a wide range of materials are considered as phase change materials with their own set of pros and cons, complicating the selection process.

2.1 Criteria for selecting a PCM

PCMs provide a much higher energy storage capability than sensible heat storage materials. In addition, the heat is stored and released at an almost constant temperature [4]. Abhat [5], Lorsch *et al.* [6] and Farid [7] developed a list of PCMs suitable for latent heat storage covering a wide range of temperatures. Not all PCMs can be used for thermal storage, but the ideal ones should exhibit the following properties [8]:

- High latent heat of fusion per unit mass, meaning a small amount of material stores a large amount of energy during the change of phase from solid to liquid.

- High specific heat provides additional sensible heat storage. Little or no super–cooling during freezing (super-cooling is the cooling of the liquid below its freezing point without it becoming a solid).
- High thermal conductivity so that the temperature gradient required for charging the storage material is small.
- A melting temperature in the desired operating temperature range.
- Non-poisonous, non-flammable, non-explosive, and not subject to chemical decomposition.
- Non-corrosive when exposed to the environment or when in contact with construction materials.
- Stability of the thermal properties over time.

Concerning the stability of properties over time, PCMs should be able to withstand a large number of cycles without degradation. Assuming that the life expectancy of the building material containing the PCM is 30 years, the thermal properties must remain constant over this time period and be able to handle 11,000 daily cycles of melting and solidification. If the PCM is encapsulated or contained, the container should exhibit comparable physical and thermal stability as the PCM. According to Gibbs and Hasnain [12], paraffins have excellent thermal stability as they do not show any degradation in their thermal behavior due to repeated recycling. No single material exhibits all the desired properties listed above. However, deficiencies can be compensated by an appropriate system design [12].

2.2 Classification of PCMs by chemical type

A large number of organic, inorganic and eutectic materials are defined based on their melting temperature and their latent heat of fusion. A classification of PCMs is shown in Figure 2.1.

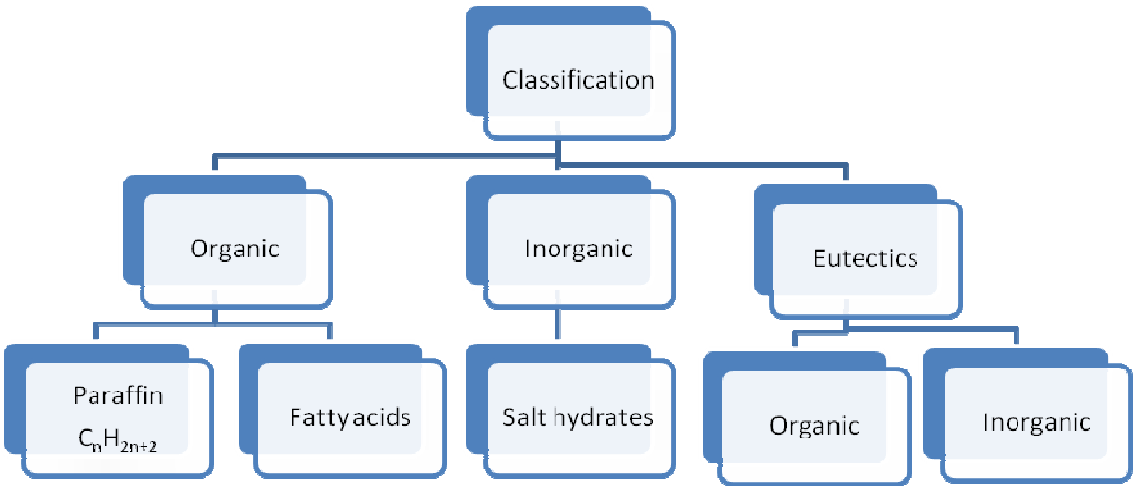

Figure 2.1: Classification of Phase change materials [13]

(i) Advantages and Disadvantages of Organic PCMs

Some of the organic PCMs used are Paraffin, 1-Teradecanol Paraffin, 1-Dodecanol Paraffin, Erythritol, High Density Polyethylene (HDPE), Palmitic acid, and Capric Acid [14]. Organic materials cover a relatively small temperature range from approximately -5^{o}C to 150°C, yet sufficient for building applications. They include fatty acids and sugar alcohol. In most cases, their density is smaller than 1g/cm^{3}. Therefore, paraffins and fatty acids usually have smaller melting enthalpies per volume than inorganic materials. Organic materials can also be mixed to modify their melting points [3, 4, 14, 15].

The characteristics of organic materials are listed below. They:

- Freeze without super-cooling,
- Exhibit the ability to melt congruently (i.e., no change in composition due to melting),
- Are self-nucleating, which speeds up solidification or crystallization,
- Do not segregate,
- Are compatible with conventional materials of construction,
- Are chemically stable,
- Exhibit a high heat of fusion, ranging from 45 to 210 kJ/kg [15],
- Are safe, non-reactive and non-toxic,
- Have low thermal conductivity in their solid state,
- Have low volumetric latent heat storage capacity,

- Are flammable, this situation can be easily addressed by a proper encapsulation or container, and
- Are relatively more expensive than other PCMs.

(ii) Advantages and Disadvantages of Inorganic PCMs:

Some of the inorganic materials used for commercial PCMs are $CaCl_2.6H_2O$, a combination of ($MgCl_2.6H_2O$, $MgNO_3.6H_2O$), $Ba(OH)_2.8H_2O$. A complete list of inorganic PCMs can be found in [13, 16]. Inorganic materials cover a wide temperature range. Their density is larger than 1 g/cm^3.

Their advantages and disadvantages are listed below. As a category they:

- Have a high volumetric latent heat storage capacities,
- Have a low cost and easy availability,
- Have high thermal conductivity,
- Have high latent heat of fusion,
- Are non-flammable,
- Exhibit super-cooling during the solid-liquid transition
- Nucleating agents are required, specifically after repeated cycling

(iii) Advantages and Disadvantages of Eutectic PCMs

Eutectic PCM are mixtures of materials with proportions that provide the lowest possible melting temperature. Some of the organic eutectic materials that can be used as

PCMs are 67% Naphtalene with 32.9% Benzoic Acid and 37.5% Urea with 63.5% acetamide. They:

- Have a sharp melting point similar to a pure substance,
- Have a volumetric storage density slightly above organic PCMs,
- Are relatively new to thermal storage applications and therefore only limited data are available on their thermo-physical properties.

2.3 Shape Stabilized and Form-Stable PCMs

Shape stabilized PCMs, innovative type of thermal energy storage materials, keep their shape during the phase change process, meaning there is no liquid phase and therefore no need of encapsulation and no risk of leakage. Their thermal conductivity, which is low, can be increased through additives with high thermal conductivity, such as ex-foliated graphite. Much research is being conducted in this area. Zhang *et al.* [13] developed a shape stabilized PCM made of paraffin with Styrene Butadiene Styrene (SBS) as the supporting material. This shape-stabilized PCM exhibits large heat of fusion.

Form-stable PCMs can be either solid-solid PCMs or solid-liquid PCMs. The materials in the solid-solid PCMs are molecular crystals that undergo transformations in their crystalline form, followed by the absorption and release of heat [17]. In addition, polymers cross-linked by adding chemical cross-linking agents or through electron beam radiation are used as solid-solid PCMs [17]. A form-stable Silane graft copolymer with a latent heat of fusion approximately 300 kJ/kg, a transition temperature of approximately

127°C and a relatively low cost has been developed [18, 19]. Although this temperature is too high for building applications, it is an example worth emulating.

The solid-liquid PCMs include compound phase change materials. In this type of shape stabilized PCMs, materials with high melting points act as supporting materials into which the PCMs are dispersed. As long as, the operating temperature is lower than the melting point of the supporting material, the compound material can keep its shape even when its state changes from solid to liquid. By infusing a porous bulk material (e.g., concrete slab) into a PCM in liquid state, a compound PCM is obtained [20].

A shape-stabilized PCM consisting of paraffin as a dispersed PCM and a HDPE as a supporting material is a new kind of compound PCM [17]. The two materials are mixed at a temperature higher than the melting point of the HDPE, and then the compound is allowed to cool. When the temperature is between the melting point of the HDPE and that of the paraffin, the HDPE solidifies while paraffin is still in its liquid state, remaining in the 3-D netted structure of the solidified HDPE. Since the HDPE has a high crystallization, the compound is strong enough even when the paraffin is liquid. Paraffin is a homologous compound of HDPE and any form of paraffin, refined or semi-refined can be mixed with HDPE easily. In the preparation of a form-stable compound, there is no chemical reaction between the HDPE and paraffin. Therefore, the latent heat of the form stable PCM is almost equal to that of paraffin in it. The form stable PCM, cheap and easy to prepare and its latent heat is comparable with traditional PCMs [17].

A new type of microencapsulated PCM (form-stable) has been developed using inorganic silica gel polymer prepared using the *in-situ* polymerization method as the coating material and form-stable paraffin as the inner material [21]. The silica gel prevents the leakage of the paraffin, and keeps the paraffin content constant.

"*Recently a novel class of fibrous polymer matrix form stable PCMs ultrafine fibers of PCM / polymer composites has been developed by electro-spinning technique* [22, 23]". Fatty acids have been the subject of extensive research in this field. Since they are non-toxic, non-corrosive, have high latent of fusion and a suitable melting temperature, they are used in solid-liquid PCMs. A series of long chain fatty acids LA, MA, PA, SA, was selected as the PCMs and the polyethylene terephthalate (PET) was selected as the polymer supporting material and the fatty acids/PET ultra-fine composite fibers were fabricated by electro-spinning [14].

Shape-stabilized PCMs can be integrated into construction materials as such or buildings can be constructed by combining PCMs with open cell cements (Thermocrete) to produce low-cost energy storage materials with structural and thermostatic properties [18].

2.4 Laboratory versus commercial grades of PCM

Few of the substances analyzed to be used as PCMs have been commercialized. Table 2.1 lists the thermo-physical properties of various PCM substances, eutectics and mixtures (inorganic, organic and fatty acids). Even though commercial grade PCMs are preferred for latent heat storage due to their availability and relatively inexpensive cost,

their thermo-physical properties and behavior have been found to be different from laboratory grade materials [24]. In addition, one cannot simply consider available data on technical grade PCMs for designing an effective heat storage device as thermo-physical properties (e.g., exact latent heat, melting temperature range, and conductivity) vary between manufacturers, primarily due to different levels of purity of the substances as well as the lack of testing by manufacturers for proprietary reasons [24].

In addition, some properties may vary when mixed with construction materials and may depend on the mixture. Hence, the properties such as conductivity, latent heat and melting temperature range need to be measured and studied.

Table 2.1. Examples of phase change materials [25]

Compound	Class	Melting Temp. (^oC)	Latent heat of fusion (kJ/kg)	Density (kg/m^3)
$Mn(NO_3)_2$ - $6H_2O$	Inorganic	25.8	125.9	1795
66.6% $CaCl_2$ - $6H_2O$ +33.3% $MgCl_2$ - $6H_2O$	Inorganic eutectic	25	127	1640
50% $Na(CH_3COO)$ - $3H_2O$ + 50% HCONH2	Inorganic mixture	40.5	255	-
1-Dodecanol	Organic	26	200	-
37.5% Urea + 63.5% acetamide	Organic eutectic	53	-	-
Capric acid	Fatty acid	32	152.7	878

2.5 Passive and active cooling systems

Based on their integration in buildings, PCMs are also categorized as passive, assisted passive and active. In the passive systems the PCMs are incorporated directly into the building for heating and cooling purposes. In the assisted passive systems, the PCMs are still incorporated in the building material, but the process of convection is used to facilitate air flow across the material surface. This ventilation is generally provided by blowers or fans. In active systems, PCMs are included in an auxiliary heating or cooling unit. The cold or the heat energy is accessed only on demand. PCMs are generally incorporated in active systems instead of being incorporated in the building construction materials, giving the advantage of being able to store the cold or the heat energy during off-peak periods for later use [26].

2.6 PCM incorporation in building materials

PCM can be incorporated into many different materials, such as gypsum wallboard, plaster, concrete, polymers, etc. By encapsulating suitable PCMs within the surfaces of walls, ceilings and floors of buildings, energy storage in those surfaces can be increased [2]. Figure 2.2 show a Scanning Electron Micrograph of a sample mixture composed of plaster (white particles) and encapsulated PCM (grey round spheres).

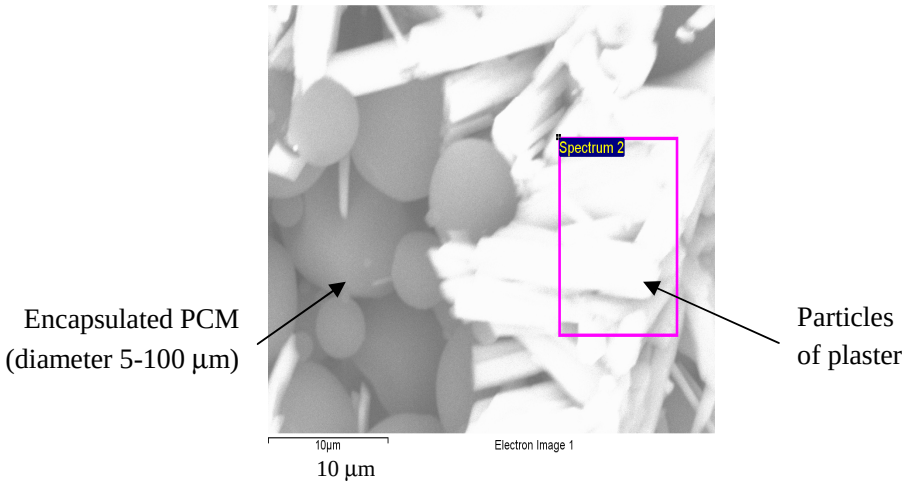

Figure 2.2: Scanning Electron Micrograph of sample mixture of plaster and PCM

Since the early 1980's several forms of encapsulated PCMs have been developed and became commercially available for active and passive solar applications including direct gain. But the surface area of these PCMs was inadequate to deliver heat to the building after the PCM was melted. In contrast the walls and ceilings of a building offer large areas for passive heat transfer within every zone of the building [2, 10]. Therefore, methods were developed for impregnating gypsum wallboard and other architectural materials with PCMs [2, 11, 27-29]. Also, methods for incorporating the PCMs into other lightweight building materials such as plywood ceiling and floor tiles were investigated.

2.7 Wallboards impregnated with PCMs

Phase change wallboard is a novel type of integrated heat storage material. Gypsum wallboards impregnated with PCMs can be installed instead of ordinary wallboards during the construction of a building. They provide thermal storage that is distributed throughout a building as a passive system and offer off-peak cooling and

heating. Peippo *et al*. [30] constructed a lightweight passive solar house (using PCM impregnated plaster board for heat storage) with an area of 120 m^2 in Madison, Wisconsin, with good insulation. A large area of glazing was facing south. The house saved up to 15 percent of the annual energy costs. Also, their study found that a PCM with a melting temperature 1 to 3°C above the average room temperature exhibited optimal diurnal heat storage.

Stetiu and Feustel also evaluated the LHS performance of PCM wall boards using a thermal simulation program based on the finite difference approach [30]. They found that thermal mass can reduce the peak power demand and therefore reduce size of the cooling or heating mechanical systems.

Neeper [11] constructed gypsum wallboard impregnated with fatty acids and paraffin waxes as PCMs. The wall was not directly illuminated by the sun, and the PCMs were subjected to the diurnal variation of the room temperature. By using a mixture of PCMs, their melting temperatures were adjusted. The three parameters of PCMs, namely (a) the melting temperature, (b) the range of melt temperature, and (c) the latent heat capacity per unit area of wall board which influences the passive absorption and release of energy during a daily cycle were studied. He found that when the melting temperature of the PCM was close to the average comfortable room temperature, maximum diurnal energy storage took place. Also, this diurnal energy storage was found to decrease when the phase change transition took place over a range of temperatures [11].

Kedll and Stovall [31] conducted their research using octadecane wax impregnated wallboard in a passive solar application. They found that full size sheets can be successfully subjected to an immersion process to fill the wallboard with wax. Through this immersion process higher storage capacity can be achieved, than by adding wax filled pellets to wall boards during manufacture.

The various applications of PCM storage in buildings can be analyzed by carrying out building energy simulations. Researchers from the Fraunhofer Institute in Germany compared the thermal behavior of different types of wall constructions incorporating different amounts of PCMs using simulations. For this an empirical model for the phase transition was developed. Wall samples having an area of 0.5 x 0.5 m^2 were used in their experiment. The research investigated how the temperature range of the phase transition, the proportion of PCMs and the structure and use of the building affected the thermal behavior of the building. The thermographs revealed the qualitative effects of the PCMs on the construction materials. Four wall samples with different amounts of PCM were heated in an oven and observed while cooling. The temperature time variation also showed the effect of PCMs. It was found that the larger the proportion of PCMs, the longer the cooling [32].

Athenitis *et al.* [33] constructed a large outdoor test room with an inner wall lined with PCM gypsum. They also conducted 1-D non-linear numerical study for this. The PCM board had 25% of PCM by weight. There was reasonable correlation between the simulation and the experimental results. It was also shown that the use of PCM gypsum

board reduced the maximum temperature by approximately 4°C during the day and could reduce the heating load at night.

Kissock *et al*. [33] used commercial paraffin K-18 in the wall boards with 30% by weight and observed the thermal behavior of the wall boards. Solar radiation, ambient temperature and interior temperatures in the test cells were continuously monitored for 14 days and simulations were run. The peak temperature recorded in the PCM test cell was approximately than 10° C lower than the one recorded in the control test cell without PCM during sunny days. These examples show the potential benefits of incorporating PCM in buildings.

CHAPTER 3

EXPERIMENTAL MEASUREMENT OF MELTING TEMPERATURE AND LATENT HEAT OF FUSION

The PCMs having a melting temperature between 15 and 40°C are recommended in building applications such that their operation temperature range matches the human comfort temperature range. A large number of PCMs are known to melt in the required range. However, this thesis focuses exclusively on encapsulated alkane hydrocarbon PCM materials, which are commonly available on the market and ready to be mixed in building construction materials. This chapter describes the experimental technique used to characterize the two most important thermo-physical properties, namely the melting temperature and latent heat of fusion.

Although the thermo-physical properties of these commercial PCMs are provided by the manufacturer, they are not provided with sufficient accuracy and confidence. Therefore, measuring them experimentally ensures that:

- we know the actual properties of the raw PCM,
- we know the properties of the PCM mixed with the construction material of interest, and
- we discover the potential effects of mixing the PCM in another material on the properties of the PCM.

3.1 Description of selected PCMs

The PCMs required for our experiments were procured from Microtek Laboratories, Inc. [34] and BASF [35]. Of the 16 types of PCMs produced by Microtek, the research study used three, namely MPCM-18D, MPCM-28D and MPCM-37D. The names of these PCMs reflect their phase change temperature of 18^{o}C, 28^{o}C and 37^{o}C, respectively. These three were selected because their phase change temperatures are appropriate for building applications. The four PCMs are encapsulated alkane hydrocarbons, Hexadecane for MPCM-18D, Octadecane for MPCM-28D, and Eicosane for MPCM-37D and the BASF Micronal product. These four products are white powder materials containing approximately 85-90 percent of PCM and 15-10 percent of a proprietary polymer shell.

3.2 Fabrication of PCM/plaster samples

The samples of PCM mixed in plaster were fabricated as follows. First a mold was built to cast samples of cylindrical shape 4" in diameter and ¾" thick. The mixture was made by mixing specific amounts of PCM powder, plaster powder and water. The casting of samples was done in three consecutive layers with drying and curing between each layer in order to avoid significant shrinkage and cracking of the samples. Each sample was dried overnight between each layer application on a hot plate at 90^{o}C. The samples were then polished using 320, 800, and 1200 grit sand paper to achieve even and parallel surfaces. The percentage of PCM was then determined by dividing the dry weight of PCM by the total dry weight of the finished sample.

Figure 3.1. Cylindrical samples made of PCM mixed in plaster

3.3 Measurement of melting temperature and latent heat of fusion

The kinetic and thermodynamic parameters of materials used as PCMs can be determined using differential scanning calorimetry (DSC). In general, when materials are heated, they undergo physical or chemical changes. Samples of about 1 to 10 mg of the material to be tested are inserted in the differential scanning calorimeter (DSC). The scanning process corresponds to heating up the sample as well as a known reference sample while measuring the instantaneous rate of heat flow (i.e., power) needed to heat up the samples. From examination of the thermograms generated by the DSC, the precise values of the phase transition temperatures during melting and solidification of the samples and the corresponding the heat of fusion can be inferred [36,37].

3.4 Interpretation of DSC Curves

Figure 3.1 shows a thermogram of a PCM-plaster mixture from -10^{o}C to 55^{o}C. A change of phase appears as a peak on the thermogram. When melting begins the sample remains at the melting temperature and absorbs heat, which corresponds to an

endothermic reaction and is shown as a negative heat flow. The solid and liquid phases are in equilibrium as melting progresses. This results in a peak whose slope reflects the rate of energy transfer to the sample, which is based on the arbitrary heating rate of the scan between 1 and 30^{o}C per minute. The thermogram of Figure 3.1 corresponds to a heating rate of 1^{o}C per minute. The magnitude of the peak indicates the end of the equilibrium melt region and the trace drops back to the baseline. After heating up the sample to a desired temperature (e.g., 55^{o}C) the scan is reversed by cooling the sample back to the initial temperature (i.e., -10^{o}C). The process of solidification is an exothermic reaction, shown as a positive peak of heat flow.

The shape of the peaks is not symmetrical and has a wider based at slow rates. The onset temperature indicates the beginning of melting. A pure material melts with a sharp and narrow peak. However due to time taken for the energy to flow into the sample the peak is broadened and reduced in height. By examining the shape of the peak purity of the sample can be estimated. The scanning rate also affects resolution and accuracy [38]. Smaller the rate, smaller is the difference between the temperatures of thermocouples of the apparatus and the actual temperature of the sample. Therefore, several tests were performed at different rates on all samples. Based on the tests at various heating rates, the melting/solidification temperature is between the peaks. As a first approximation, the average between the two peak temperatures can be used.

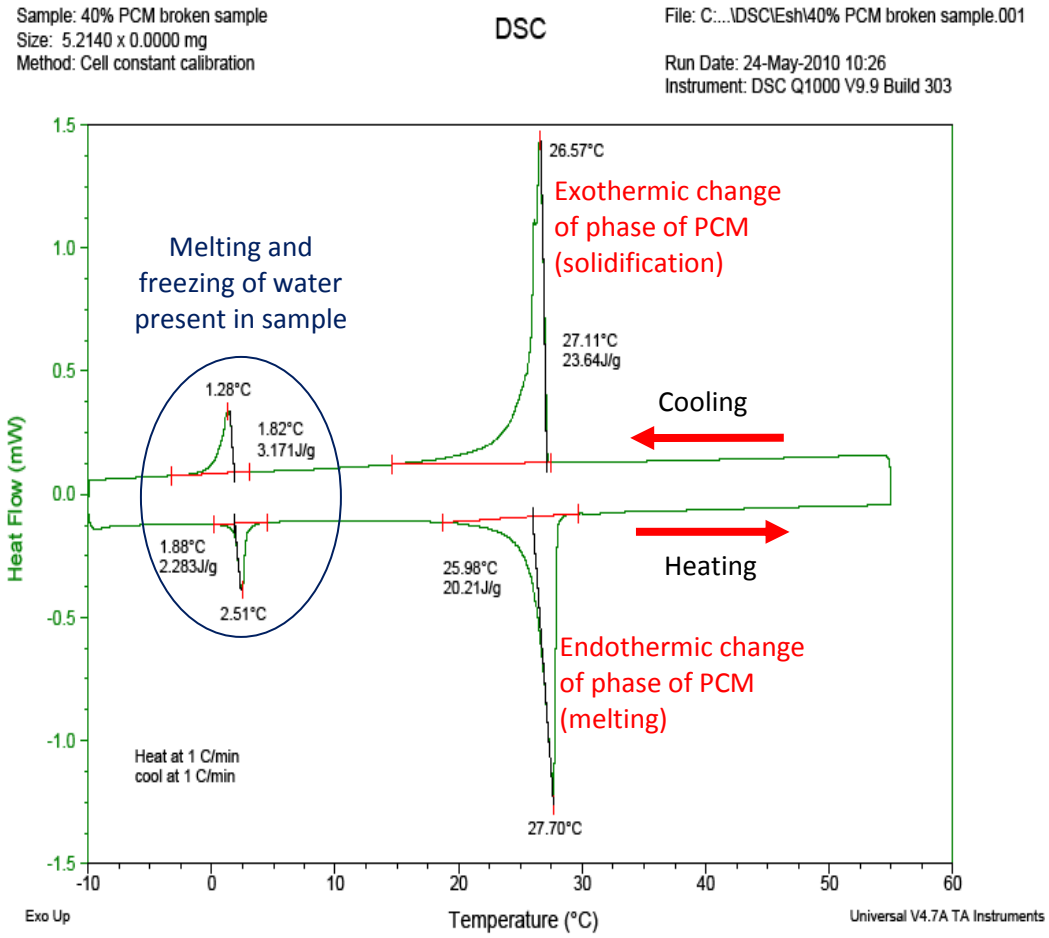

Figure 3.2: DSC Curve for 40% PCM-Plaster Sample @ 1°C/ min

DSC and other Differential Thermal Analysis (DTA) methods of analysis have their limitations, including [39]:

1) The instrumentation is complex and expensive,
2) Only small portions of any given sample can be analyzed, which may prevent capturing macro-scale heterogeneity in the sample,
3) The actual change of phase cannot be visually observed.

When the peak is sharp and well defined for both the endothermic process (heating) and the exothermic process (cooling), the corresponding slope of the curve indicates that the rate of flow is relatively fast. The heat of fusion can be determined by multiplying the area under the peak curve by the calorimetric constant of the calorimeter. This calculation is generally done internally and the result is provided on the thermogram.

3.5 DSC results

The three encapsulated alkane hydrocarbon PCMs from Microtek (MPCM-18D, MPCM-28D and MPCM-37D) were tested individually as well as a PCM-plaster mixture (40%wt MPCM-28D with 60%wt plaster, dry weight) at various heating and cooling rates. All results are available in Appendix B. This section presents the results pertaining to MPCM-28D, whose melting temperature is reported to be 28^{o}C.

Mixed PCM/Plaster sample

Table 3.1 summarizes the results of the DSC, namely the transition temperature and the latent heat, for a PCM-plaster mixture with 40%wt PCM for various heating and cooling rates from 1^{o}C/min to 30^{o}C/min. The corresponding averages and standard deviations for both endothermic and exothermic processes provide a good estimation of these thermal properties.

Table 3.1: DSC results for PCM plaster mixture sample (40%wt of PCM-28D) for different heating rates

Scan Rate (°C /min)	**Phase Change Temp. (°C)**	**Latent Heat (J/g)**	**Phase Change Temp.(°C)**	**Latent Heat (J/g)**
	Endothermic Process		**Exothermic Process**	
1	27.96	20.21	27.11	23.64
8	26.13	22.03	26.84	22.10
15	26.27	22.33	26.74	22.81
23	26.35	21.55	26.62	22.23
30	26.28	21.21	26.50	22.61
Avg.	26.60	21.47	26.76	22.67
St. dev.	0.77	0.82	0.23	0.61

Pure PCM sample (MPCM-28D)

A pure PCM sample of Microtek MPCM-28D was tested. The shape of the curves is similar for all scanning rates. As shown in Figure 3.3, the endothermic curve (melting) has a single primary peak and the exothermic curve (solidification) has a primary peak and a secondary peak.

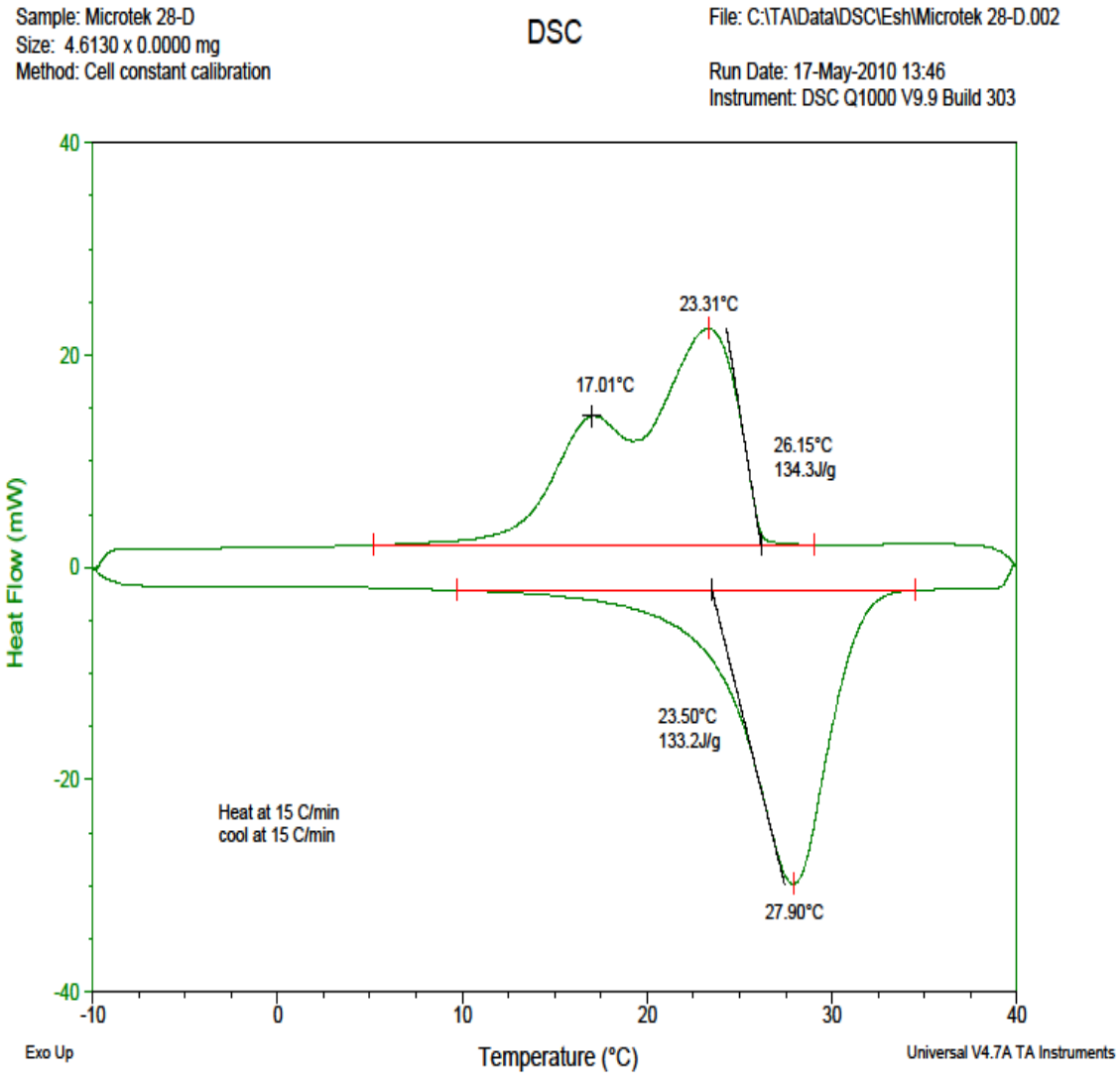

Figure 3.3: DSC Curve for pure Microtek MPCM-28D Sample @ 15°C/ min

Table 3.2. DSC results for MPCM-28D at different heating rates

Scan Rate (°C/min)	Type of process	Phase Change Temp. (°C)	Latent Heat (J/g)
1	Endothermic	23.48	127.2
	Exothermic	26.40	134.4
15	Endothermic	23.50	133.2
	Exothermic	26.15	134.3
23	Endothermic	23.58	133.4
	Exothermic	25.99	134.8
30	Endothermic	23.32	137.1
	Exothermic	25.98	136.8

Under all heating rates, the peak is sharp and well defined for both the endothermic process (melting). The exothermic process (solidification), however, shows two peaks at two different temperatures. This phenomenon is speculated to be due to nucleation of the PCM inside each capsule during solidification, which results in a non-uniform thermal conductivity and two peaks. However, more investigation must be done to fully explain the presence of these two peaks since they do not appear on the thermogram of the PCM/plaster mixture.

While the exothermic phase change temperature is in accordance with the temperature provided by the manufacturer, the endothermic temperature is not. This is also due to the phenomenon mentioned above with the presence of the two peaks.

As shown in Appendix B, the other two PCM products show the same phenomenon with two peaks very close to each other for MPCM-18D, and three peaks for MPCM-37D.

In terms of latent heat, comparing the mixed PCM/plaster sample to the pure PCM sample shows a discrepancy. The measured latent heat of the mixed PCM/plaster sample is 22.7 J/g. Since it includes 40%wt PCM, it should have a latent heat corresponding to about 40% of the latent heat of the pure PCM sample, which is 40% of 135.1 J/g. The expected latent heat of the mixed sample would be 0.4*135.1 = 54.0 J/g. This discrepancy is speculated to be due to the non-uniform distribution of PCM throughout the mixture. Since only a small portion of the PCM/plaster sample is tested (i.e., piece of 5.2 mg broken off the sample of 30 g), it may not be representative the entire sample. This should be easily verified by testing several pieces from the same sample and show that the measured latent heat varies significantly between pieces of the same sample and that the average value corresponds to the expect value.

CHAPTER 4

EXPERIMENTAL MEASUREMENT OF THERMAL CONDUCTIVITY

The ASTM standard titled ”Standard Test Method for Steady State Thermal Transmission Properties by Means of Heat Flow Apparatus” [40] was used as a base for determining the thermal conductivity of PCM/plaster samples. The standard is used to measure the thermal conductivity of samples by measuring the heat flux and temperature gradient through a thermopile.

4.1 Experimental Procedure

The following equipment was used in the experiment:

- A hot plate as the heat source,
- A beaker with ice water as heat sink (cold source),
- Two Omega® HFS-3 model heat flux transducers (sensors) with integrated thermocouple of Type K,
- A Analog/Digital Input/Output InstruNET® data acquisition system to record temperature and heat flux data as function of time,
- High temperature high thermal conductivity paste (Omegatherm 201) placed between the sample, the hot plate, the beaker, and sensors as shown in Figure 4.1 in order to mitigate the effect of poor physical contact between all parts of the thermopile, and

- Styrofoam insulation around the sample for thermal insulation. The insulation ensures that most of the heat that enters the sample from the heat source comes out of the sample into the heat sink.

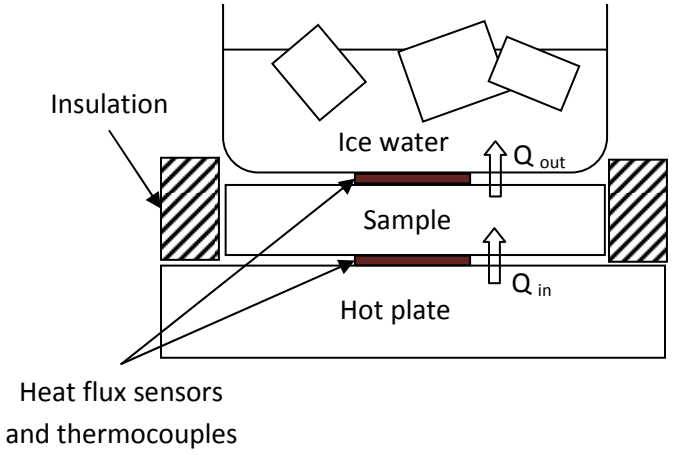

Figure 4.1. Experimental setup

The temperature of the hot plate was maintained at a set temperature (i.e., 90°C and 45^{o}C for measuring the conductivity at two different temperatures) and the temperature of the ice water was maintained at 0^{o}C. As shown in Figures 4.2, the sample was placed on top of the hot plate and below the ice water beaker. Two heat flux sensors with integrated thermocouples were placed between the sample and the heat source and sink. High conductivity paste was inserted between the sensors, samples and heat source and sink to ensure proper heat transfer. The sensors were then connected to the external channels of the data acquisition system.

The same procedure was repeated for two samples. Sample A was made of 100 percent plaster. Sample B was made of 13 percent by weight of MPCM-28D following the fabrication process described in Section 3.2.

Temperature and heat flux were recorded over time for both sides of the sample until steady state was reached. The data was then plotted and analyzed.

Figure 4.2. Thermal conductivity experimental setup (left) and data acquisition system (right)

4.2 Calculation of thermal conductivity

The temperature difference (ΔT) between the two sides of the sample and the heat flux values are used to determine the conductance, C, and conductivity, λ, as defined in the ASTM standard [51]:

$$C = S*E*L/\Delta T \quad (1)$$

$$\lambda = C/L = S*E/\Delta T \quad (2)$$

where E is heat flux transducer output (voltage), L is the sample thickness and S is a calibration factor of the heat flux transducers. The calibration factor is generally assumed to be a constant that depends on the experimental setup [40]. Since S is unknown,

equations (1) and (2) are used to directly compare the conductance and conductivity of sample B with those of sample A. Using indexes A and B referring to samples A and B, respectively, the ratios of conductance and conductivity are:

$$C_B / C_A = (E_B * L_B * \Delta T_A)/(E_A * L_A * \Delta T_B) \quad (3)$$

$$\lambda_B / \lambda_A = (E_B * \Delta T_A)/(E_A * \Delta T_B) \quad (4)$$

4.3 Analysis of results

The first step was to calibrate the heat flux sensors to verify that they provide similar readings by placing them between the hot and cold sources without sample. As shown in Figure 4.4, both sensors output the same voltage as function of time within about 0.1 mV and a discrepancy of 5.5% in streaming time. Since we are interested in steady state values, the time-averaged values (shown as straight lines in Figure 4.4) are more appropriate for this purpose. The time-averaged values differ by 0.025 mV or 1.4%, which is assumed to be acceptable.

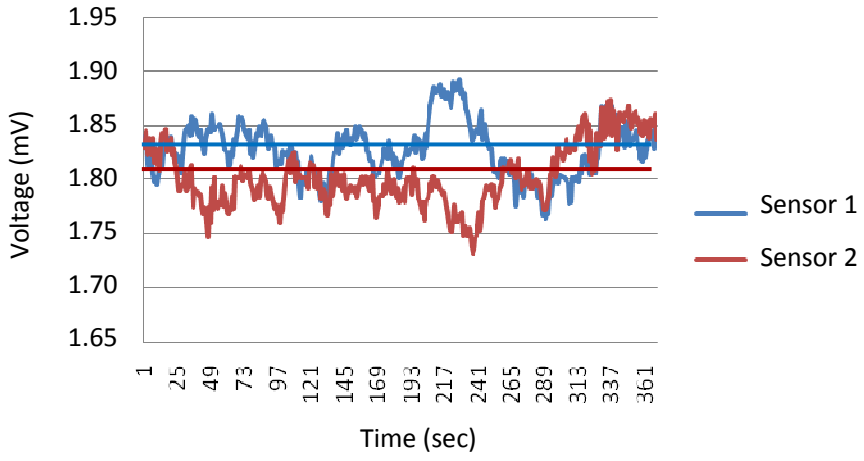

Figure 4.3 Calibration of heat flux sensors without sample

Two samples were tested with different concentrations of PCM: 0% and 13%. Both samples were tested following the same procedure with two different temperature settings for the hot source: 90^{o}C and 45^{o}C. The results for the two samples are shown graphically in this chapter.

Figure 4.5 and Figure 4.6 show the heat flux and temperature data, respectively, for the 100% plaster sample for the two temperature settings (i.e., 90^{o}C and 45^{o}C). Figure 4.5 shows that a steady state is reached where both heat flux sensors converge to the same value. This suggests that most of the heat travels directly from the hot source to the cold source through the sample without much heat loss through the sides of the sample. Also, as expected, the heat flux is much greater with the larger temperature gradient induced by the 90^{o}C hot source setting. The second figure also shows that steady state is reached, at which the temperature gradient through the sample can be measured.

Similarly, Figures 4.7 and 4.8 show the results for the 13% PCM sample for the two hot source temperature settings. In all cases, the steady state is reached where the two heat fluxes converge to the same value.

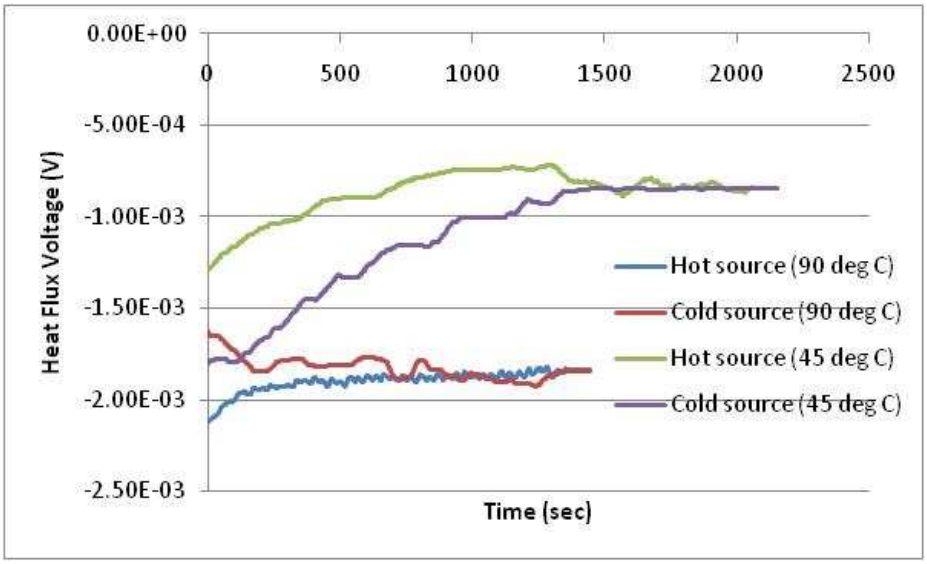

Figure 4.4. Heat flux data for the 100% plaster sample for the two hot source temperature settings (i.e., 90°C and 45°C)

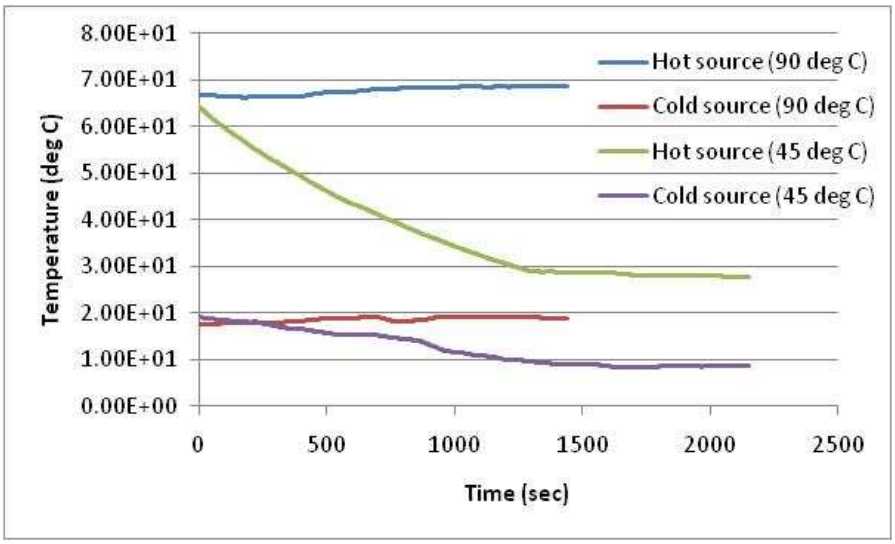

Figure 4.5. Temperature data for the 100% plaster sample for the two hot source temperature settings (i.e., 90°C and 45°C)

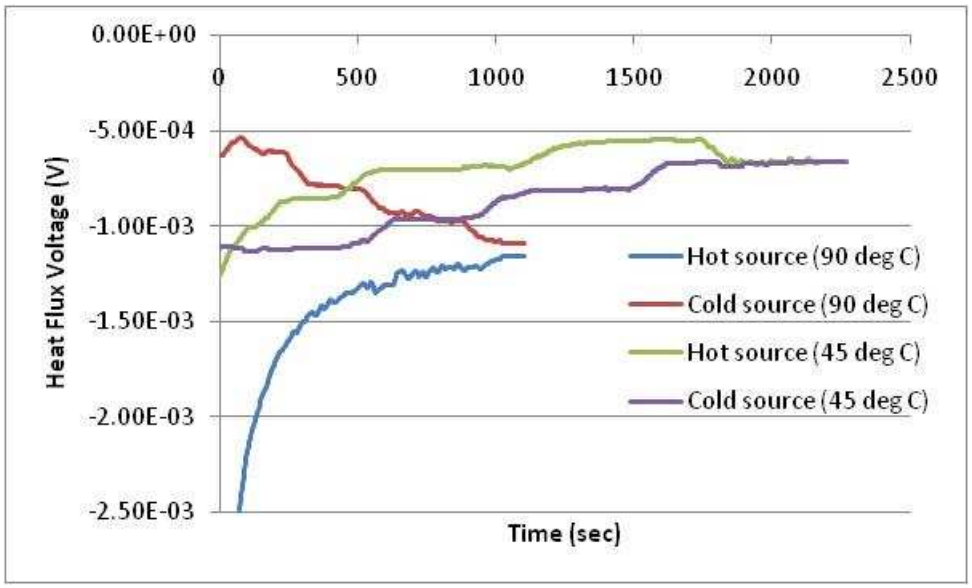

Figure 4.6. Heat flux data for the 13% PCM sample for the two hot source temperature settings (i.e., 90°C and 45°C)

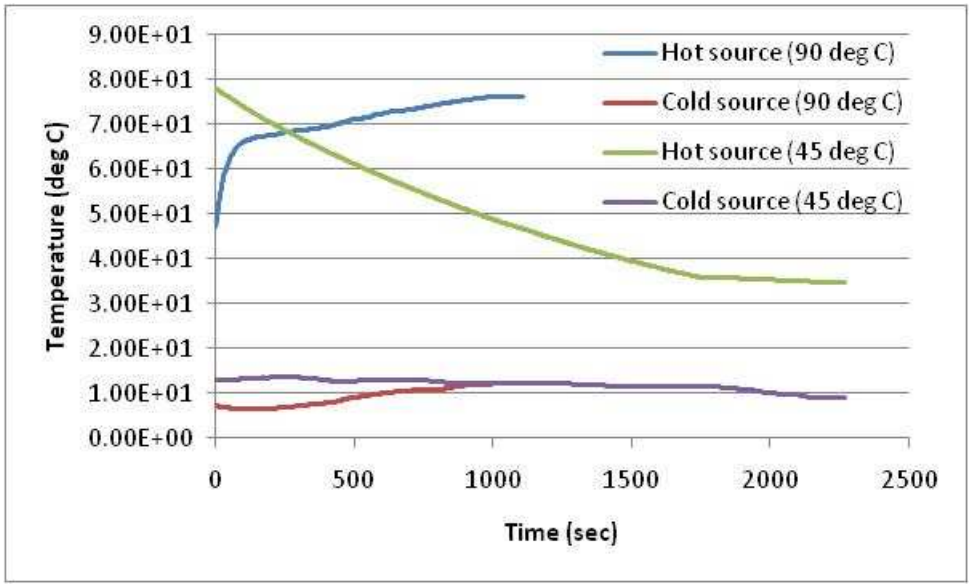

Figure 4.7. Temperature data for the 13% PCM sample for the two hot source temperature settings (i.e., 90°C and 45°C)

The steady state values can now be used in equations (3) and (4) to calculate the ratio in conductance and conductivity between the 100% plaster sample and the 13% PCM sample.

Table 4.1. Summary of results comparing 13% PCM sample to 100% plaster sample

		90^oC setting	45^oC setting
Sample A (100% plaster)	E_A (V)	-1.82e-3	-0.84e-3
	ΔT_A (deg C)	50.5	18.0
	L_A (mm)	15.0	15.0
Sample B (13% PCM)	E_B (V)	-1.16e-3	-0.64e-3
	ΔT_A (deg C)	64.5	25.5
	L_B (mm)	20.0	20.0
$C_B / C_A = (E_B * L_B * \Delta T_A)/(E_A * L_A * \Delta T_B)$		0.665	0.717
$\lambda_B / \lambda_A = (E_B * \Delta T_A)/(E_A * \Delta T_B)$		0.499	0.538

Table 4.1 summarizes the results of the comparison between the two samples in terms of conductance C and conductivity λ. The conductance values depend on the thickness of the samples. Since the thicknesses of the samples are different, the thermal conductivity value is a more valuable property. The results of the 90^oC hot source setting suggest that the conductivity of the 13% PCM sample is 49.9% of that of the 100% plaster sample. This percentage increases to 53.8% for the 45^oC hot source setting. This discrepancy is probably due to experimental error, measurement inaccuracies, and possibly the effect of phase change in the 13% PCM sample. Based on these results, it appears that the PCM acts as a significant insulator.

In order to generalize this result, statistical significance should be achieved by testing more than one sample. In addition, various concentration of PCM should be tested under various temperatures conditions. In particular, the conductivities of the sample at temperatures below and above the melting temperature of the PCM should be measured and compared.

CHAPTER 5

NUMERICAL SIMULATION

The goal of the numerical Finite Element Analysis (FEA) is to evaluate potential energy savings when incorporating PCM in building plaster wallboards. The software that is adopted for the numerical analysis is Abaqus 6.8 [41]. This FEA software helps in the numerical verification of whether the PCMs can be effectively incorporated into building for reducing heating and cooling loads. Commercial architectural software such as Design Builder [42] and Energy Plus [43] can also be used for this type of analysis. However, they not provide the heat transfer details needed for this study. Instead, they provide general information from an architectural point of view on energy consumption of a given building over long periods of time such as days, months and years. In addition, Design Builder does not provide the freedom to define the thermal and physical properties of PCM. Alternatively, Abaqus can be used to describe the detailed heat transfer mechanism that takes place during heating and cooling of specific building and wall assemblies, which is more appropriate for this study.

5.1 Numerical model

The model consists of a four-layer assembly (Figure 5.1), which is subjected to indoor and outdoor boundary conditions. Although these conditions are academic, they are realistic representations of actual effects of the heating, ventilation and air

conditioning (HVAC) that would occur on a building facade with solar radiation, thermal radiation and convection.

Although the model is defined in the three-dimensional space, the heat transfer problem is one-dimensional, which may be solved using analytical means or finite difference numerical methods. However, the ultimate goal is to expand this FEA model to a full three-dimensional heat transfer problem at the scale of a building room or zone.

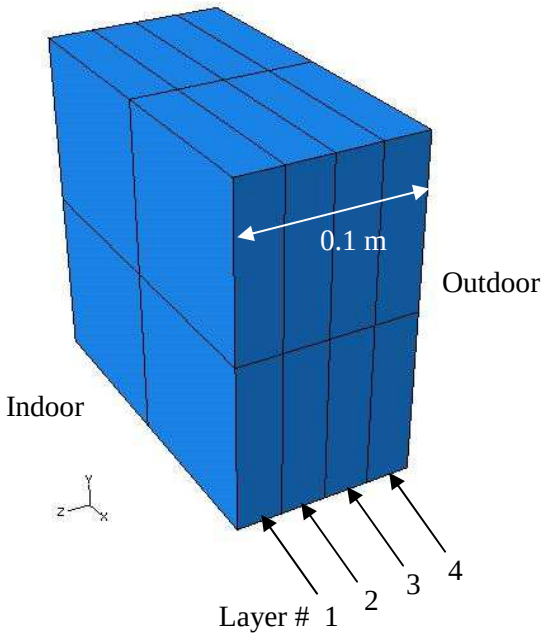

Figure 5.1. Geometry of wall panel 0.2 m x 0.2 m x 0.1 m

The wall is partitioned through the thickness into four layers in order to easily defined specific material properties for each layer corresponding to various PCM concentrations. The PCM is assumed to have a melting temperature of 20^{o}C. In Abaqus®, the melting and solidification processes are assumed to occur between the liquidus and solidus temperatures, which correspond to the onset of melting and solidification. In the

present case, these temperatures are set to +/- 2^{o}C from the melting temperature, i.e, liquidus temperature is set to 18^{o}C and the solidus temperature in set to 22^{o}C. In this range, the ratio of liquid phase over solid phase is proportional to temperature. For instance, at a given node, if the temperature is 18^{o}C, the phase is solid. At 20^{o}C, the phase is fifty percent solid and fifty percent liquid, and the stored heat is fifty percent of the latent heat per unit mass of PCM. Similarly, at 22^{o}C, the phase is entirely liquid and one hundred percent of the latent heat is stored in the material. This difference between liquidus and solidus temperatures is also a means to account for the time lag for the heat to penetrate through the thickness of the PCM polymeric capsule and reach the actual PCM chemical.

5.2 Operating conditions

The numerical analysis corresponds to a transient heat transfer analysis under various initial conditions and boundary conditions.

Initial condition: The temperature of the entire model is set to 20^{o}C at t = 0 sec.

Temperature boundary conditions: The indoor wall is set to T_1 = 20^{o}C for the entire duration of the simulation, which is the desired indoor temperature for thermal comfort. No temperature boundary condition is specified on the other walls of the model, which means that the exterior wall surface temperature will vary based on the heat flux applied on the surface.

Reaction heat flux: By prescribing the temperature of the indoor wall, it is assumed that the active heating and cooling system of the building is used to maintain this prescribed wall temperature by means of a thermostat. For instance, if the temperature of the wall

were to increase above 20°C, the thermostat would turn the air conditioning on, which would remove the heat stored in the wall in order to maintain the wall temperature at 20°C. In the numerical simulation, this action is created by a reaction heat flux, Q_R, applied on the indoor wall. This reaction heat flux is calculated during the simulation and provides a direct quantification of energy consumption.

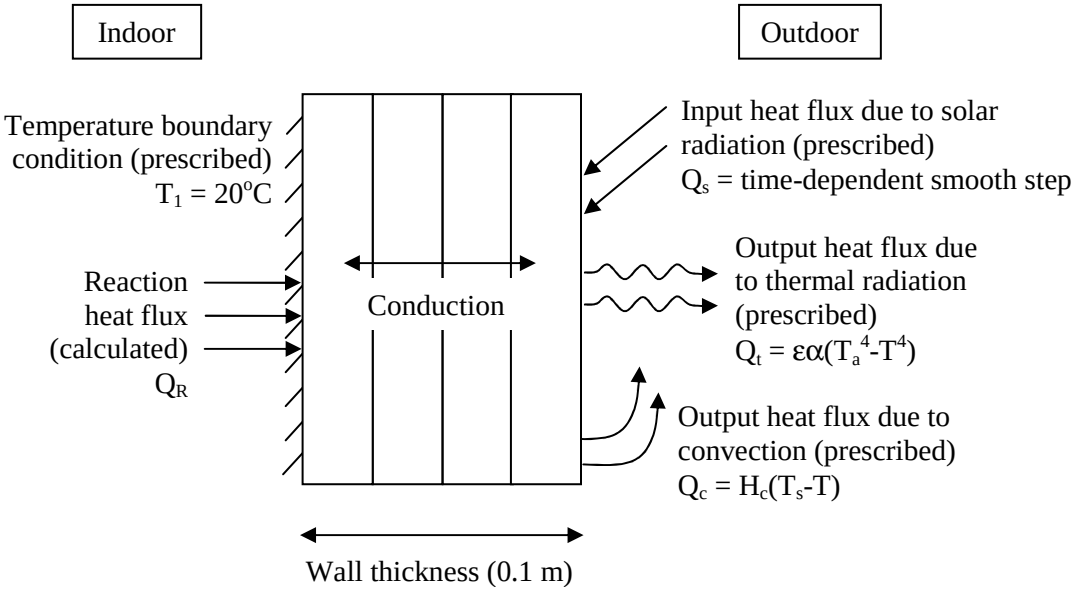

Figure 5.2. Heat transfer phenomena in wall panel

Applied loads: Three loads are applied on the outdoor wall:

- Solar radiation heat flux (W/m^2), $Q_s = Q_{s0}(1+\sin(\omega t))$, where t is time (sec), ω is the circular frequency (rad/s), and Q_{s0} is the magnitude of solar radiation (W/m^2).
- Thermal radiation heat flux (W/m^2), $Q_t = \varepsilon\alpha(T_a^4 - T^4)$, where T is the temperature of the wall surface (K), T_a is the ambient temperature of the environment facing

the surface (K), $T_a = T_{a0} - T_{a1}\cos(\omega t)$, ε is the emissivity of the surface and α is the Stefan-Boltzmann constant, $\alpha = 5.67e\text{-}8\ W/m^2K^4$.

- Convective heat flux due to convection, $Q_c = H(T_s - T)$, where H is the heat transfer coefficient (W/m^2K), T_s is the temperature of the air in contact with the wall exterior surface, $T_s = T_{s0} - T_{s1}\cos(\omega t)$, and T_{s0} and T_{s1} are two constants that define the time variations of the air temperature.

Materials used for the simulation

Four cases summarized in Table 5.1 are analyzed and compared:

(1) 100 percent plaster,

(2) plaster with 20 percent by weight of PCM and high conductivity,

(3) plaster with 20 percent by weight of PCM and low conductivity,

(4) plaster with 80 percent by weight of PCM and low conductivity.

Table 5.1 Thermo-physical properties of PCM mixtures used in numerical model

Material	Density (kg/m^3)	Conduct. (W/mK)	Specific Heat (J/gK)	Latent heat of Fusion (J/g)	Solidus Temp. (^oC)	Liquidus Temp. (^oC)
100% Plaster	700	0.17	1.0	-	-	-
20% PCM High Conduct.	700	0.17	1.0	40	18	22
20% PCM Low Conduct.	700	0.10	1.0	40	18	22
80% PCM High Conduct.	700	0.17	1.0	160	18	22

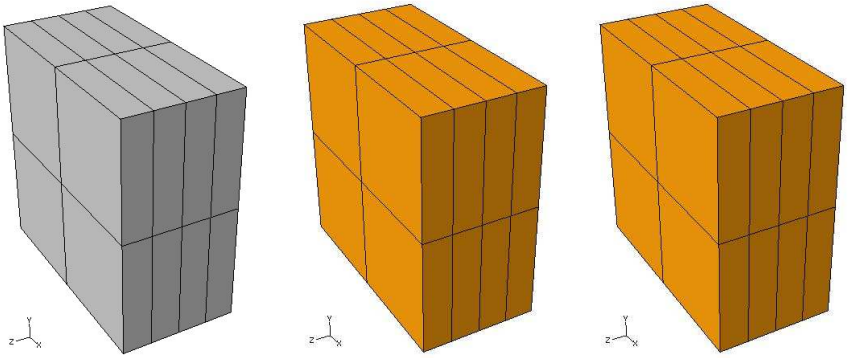

Case # 1:
100% plaster
λ = 0.17 W/m K

Case # 2:
20% PCM
λ = 0.17 W/m K

Case # 3:
20% PCM
λ = 0.10 W/m K

Figure 5.3: Parametric study of effect of PCM and conductivity

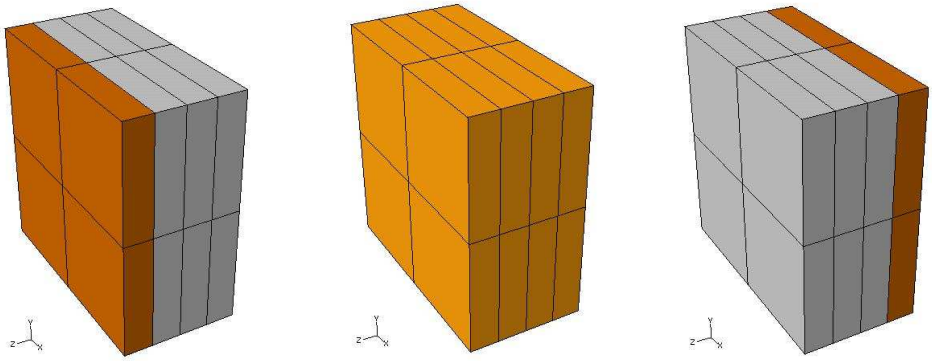

Case # 1:
80% PCM in layer 1
100% plaster in layers 2 to 4

Case # 2:
20% PCM in all layers

Case # 3:
80% PCM in layer 4
100% plaster in layers 1 to 3

Figure 5.4: Parametric study of effect of location of PCM

5.3 Results

All analyzes are run for 2000 seconds to simulate an accelerated heating and cooling cycle.

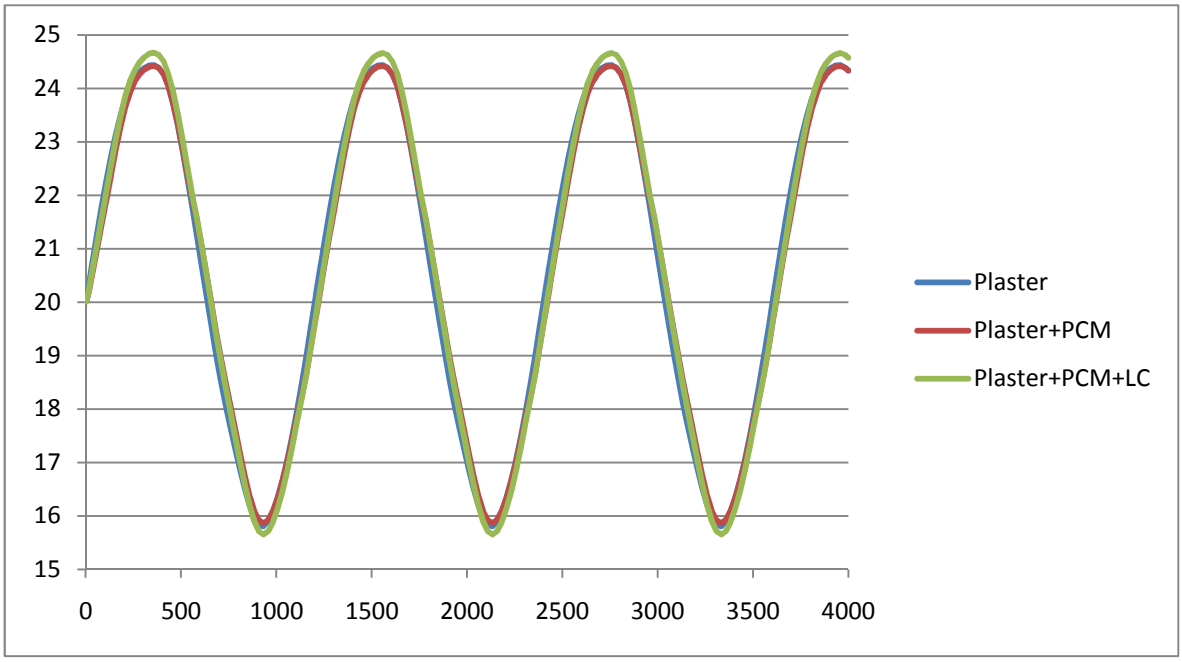

Figure 5.5: Effect of PCM and conductivity

Figure 5.5 reveals the effect of PCM on temperature distribution when the plaster, plaster combined with PCM or plaster combined with low conductivity PCM is taken into account.

Figure 5.6 reveals the heat flux distribution for the three different cases when ever plaster is taken alone or when both plaster and PCM are combined and in the third case being when the plaster is combined with low conductivty PCM. The desired distribution will be mostly when the curves are distibuted over a larger range of time period.

The second case that is being analyzed is basically how the energy consumption is affected with regard to the location of the PCM. This variation is generally done by carrying out the variation of the nodal temperature and the reaction heat flux.

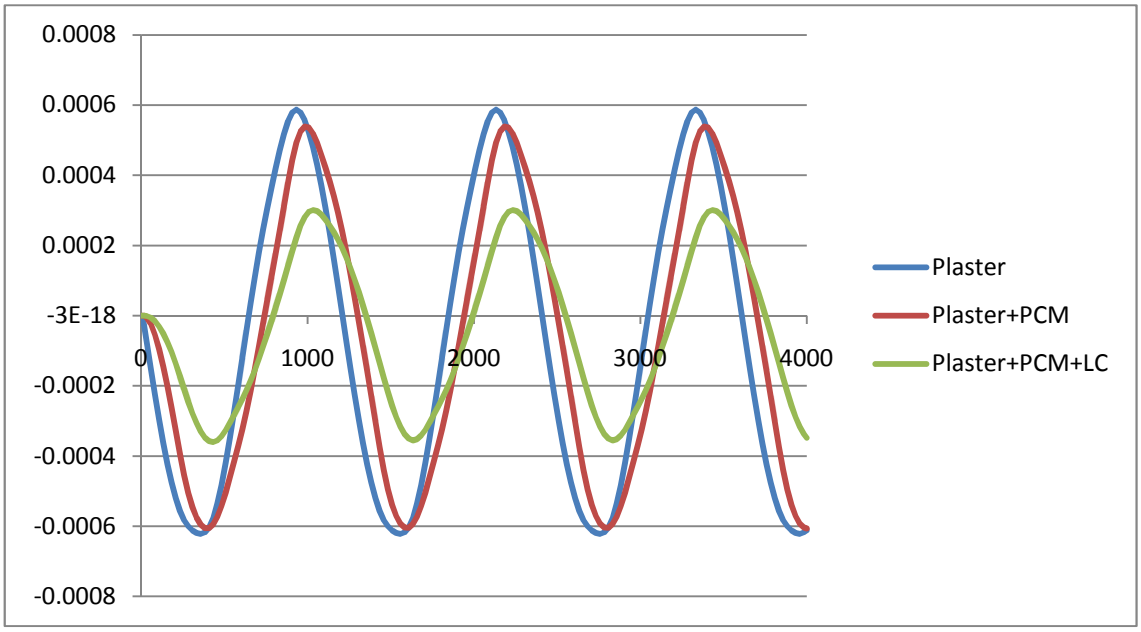

Figure 5.6: Reaction heat flux as function of time for plaster, plaster+PCM and plaster combined with low conductivity PCM

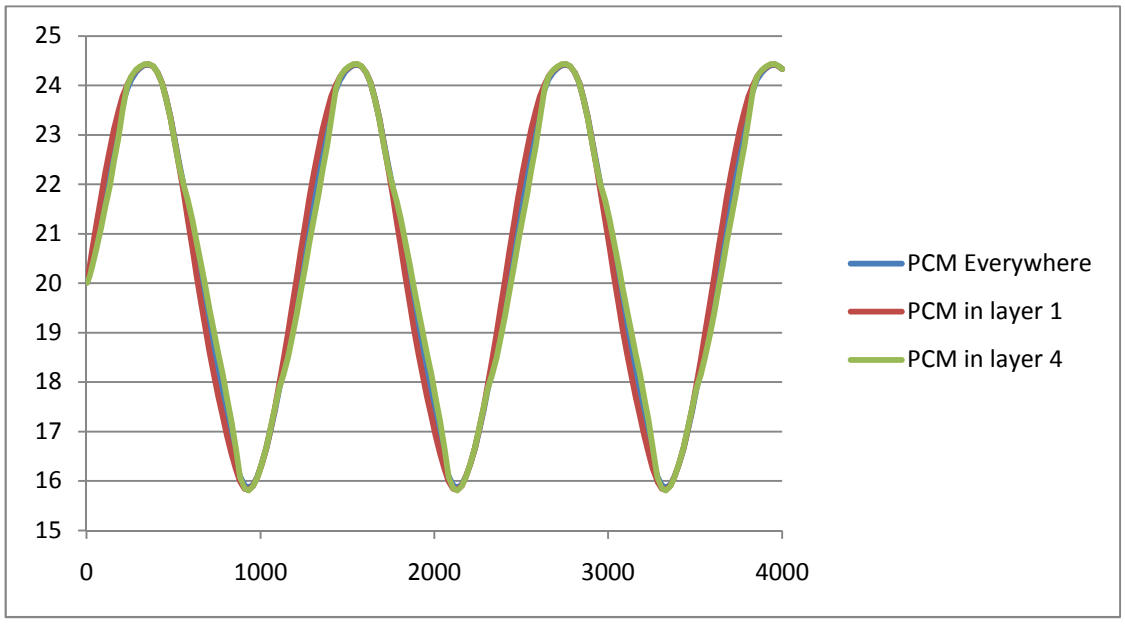

Figure 5.7: Temperature variation when the location of the PCM is varied

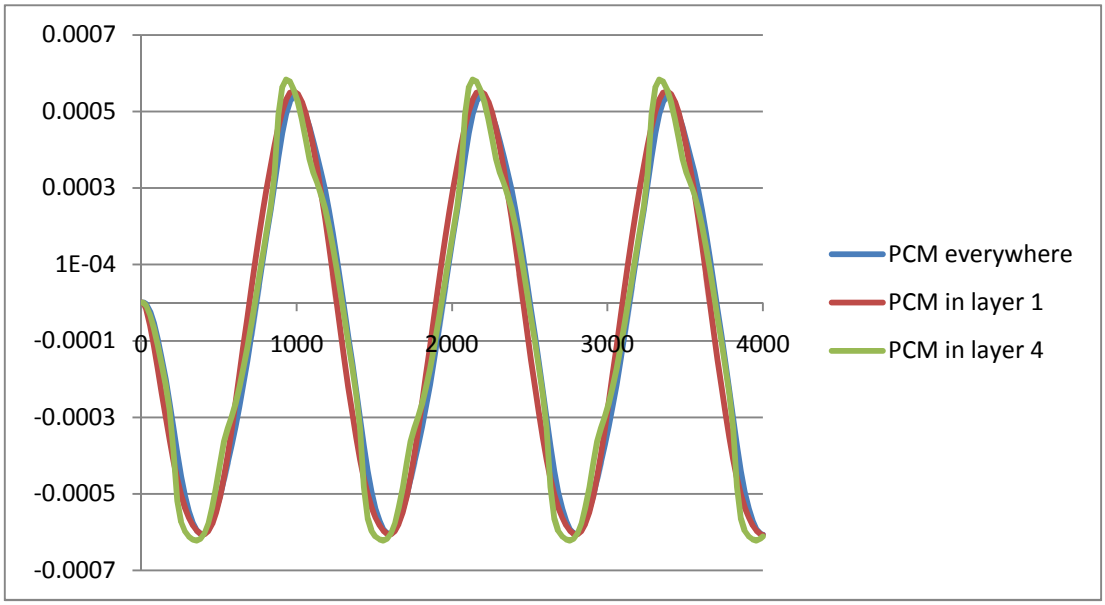

Figure 5.8: **Reaction heat flux variation when the location of PCM is varied**

From Figure 5.7 we observe that the temperature variation does not get affected by the location of the PCM in contrast to the type of the PCM that is used. Similarly rhe heat flux reaction also does not get affected whenever the location of the PCM is changed. The desired distribution of theheat flux reaction over the time period is also not observable in contrast to the type of PCM that is used.

From the Figures 5.5 to 5.8, it is found that the total energy reaction, total energy residual and the total energy input were different when the PCMs were placed on the first and the fourth layers of the four walled structure. This clearly indicates that the location of PCM does affect the energy consumption i.e., the presence of PCM reduces the energy consumption.

CHAPTER 6

CONCLUSION AND FUTURE WORK

6.1 Conclusion

The objective of the thesis was to study phase change materials (PCM) for integration into building construction materials such as plaster. A review and classification of existing PCM were done based on the literature with a list of characteristics of each material. The experimental characterization of the thermal properties of plaster samples with PCM was performed in order to assess how the integration of PCM in building construction materials affects properties. The measured properties are the phase change temperature, the latent heat and thermal conductivity. These properties are necessary in any numerical model that would be used in design. A numerical model of a wall assembly was developed and used to understand the effect of latent heat and conductivity on the performance of buildings by means of parametric studies.

The experimental study included:

- The preparation of PCM samples with desired composition.
- Determination of the phase change temperature and latent heat by conducting Differential Scanning Calorimetry (DSC) analysis. This analysis highlighted the differences between measured properties and the properties provided by the

manufacturer. It also revealed unexpected phenomena that are yet to be explained such as the appearance of several energy peaks corresponding to different temperatures during the cooling process of PCM.

- Determination of the thermal conductivity of a PCM/plaster mixture sample relative to the conductivity of pure plaster using a thermopile experiment. Based on the results, the presence of PCM significantly reduces the conductivity.

- Highlighting the limitation of the current experimental set up viz.

    - Only when both the HFS sensors are exactly identical the difference in their readings will indicate the actual difference in the experimental observation (Thermoelectric Voltages) due to the position of the sensors.

    - The insulation is not effective and the sample is not fully insulated from heat.

- Development of numerical model for inclusion of PCMs in four walled structure.

DSC Analysis showed that:

- Microtek 28D PCM is the best candidate to be used for passive storage for living and working quarters.

- Microtek 37D is the best candidate to be used for central storage systems.

- For 40 % PCM, the transition points viz. 26.5 °C and 26.28°C fall in the range of comfort zone temperature confirming its suitability for incorporation in buildings.

- The tests provide accurate quantification of latent heat (give values for the 3 PCM products), and the melting/crystallization temperature (give values for the 3 PCM products).

- The shape of the curves provide an estimation of possible impurities. In particular, two peaks are shown in crystallization curves of Microtek 28D and Mcirotek 37D. It is still not clear what they are but we are now aware of their presence.

Thermal conductivity experiment showed that The value of thermal conductivity for 13% PCM is less than that of 100% Plaster.

6.2 Future work

Based on the work carried out the following suggestions are made for future investigations in the field:

- Identical HFS with greater sensitivity will yield better and reliable results
- More sophisticated and better moulds can be procured instead of being made for the preparation of PCMs for research so that the finish is better with no material loss on the periphery of the sample. This fact being supported by the DSC curve taken for 40% PCM

- A proper insulation is recommended instead of the Styrofoam used for the insulation
- The thermal properties of the PCMs could be improved (by selecting appropriate additives to meet specific purpose for which they are used) based on the results obtained in the thermal (DSC Analysis)
- The work done enables to draw a set of design guidelines for which the results obtained from thermo-electric characterization and numerical simulation can act as input.

APPENDICES

APPENDIX A

LIST OF COMMON PHASE CHANGES MATERIALS

Table A.1: Inorganic substances [25]

Compound	Melting temperature (°C)	Heat of fusion (kJ/kg)	Thermal conductivity (W/m K)	Density (kg/m^3)
H_2O	0 [1,5]	333 [1] 334 [5]	0.612 (liquid, 20 °C) [1] 0.61 (30 °C) [5]	998 (liquid, 20 °C) [1] 996 (30 °C) [5] 917 (solid, 0 °C) [1]
$LiClO_3 \cdot 3H_2O$	8.1 [6,7]	253 [6]	n.a.	1720 [6]
$ZnCl_2 \cdot 3H_2O$	10 [8]	n.a.	n.a.	n.a.
$K_2HPO_4 \cdot 6H_2O$	13 [8]	n.a.	n.a.	n.a.
$NaOH \cdot 3\frac{1}{2}H_2O$	15 [8] 15.4 [7]	n.a.	n.a.	n.a.
$Na_2CrO_4 \cdot 10H_2O$	18 [8]	n.a.	n.a.	n.a.
$KF \cdot 4H_2O$	18.5 [1,6,7,9]	231 [1,6,9]	n.a.	1447 (liquid, 20 °C) [1] 1455 (solid, 18 °C) [1] 1480 [6]
$Mn(NO_3)_2 \cdot 6H_2O$	25.8 [18]	125.9 [10]	n.a.	1738 (liquid, 20 °C) [10] 1728 (liquid, 40 °C) [10] 1795 (solid, 5 °C) [10]
$CaCl_2 \cdot 6H_2O$	29 [4,11]	190.8 [4,11]	0.540 (liquid, 38.7 °C) [4,11]	1562 (liquid, 32 °C) [4,11]
	29.2 [7]	171 [1,9]	0.561 (liquid, 61.2 °C) [11]	1496 (liquid) [1]
	29.6 [6]	174.4 [12]	1.088 (solid, 23 °C) [4,11]	1802 (solid, 24 °C) [4,11]
	29.7 [1,9]	192 [6]		1710 (solid, 25 °C) [1]
	30 [8]			1634 [12]
	29–39 [12]			1620 [6]
$LiNO_3 \cdot 3H_2O$	30 [6]	296 [6]	n.a.	n.a.
$Na_2SO_4 \cdot 10H_2O$	32.4 [1,7,9]	254 [1,9]	0.544 [1]	1485 (solid) [1]
	32 [13]	251.1 [12]		1458 [12]
	31–32 [12]			
$Na_2CO_3 \cdot 10H_2O$	32–36 [12]	246.5 [12]	n.a.	1442 [12]
	33 [6,7]	247 [6]		
$CaBr_2 \cdot 6H_2O$	34 [4,7,11]	115.5 [4,11]	n.a.	1956 (liquid, 35 °C) [4,11]
				2194 (solid, 24 °C) [4,11]
$Na_2HPO_4 \cdot 12H_2O$	35.5 [8]	265 [12]	n.a.	1522 [12]
	36 [12]	280 [6]		
	35[6,9]	281 [9]		
	35.2 [7]			
$Zn(NO_3)_2 \cdot 6H_2O$	36 [4,7,11]	146.9 [4,11]	0.464 (liquid, 39.9 °C) [4,11]	1828 (liquid, 36 °C) [4,11]
	36.4 [1,9]	147 [1,9]	0.469 (liquid, 61.2 °C) [7]	1937 (solid, 24 °C) [4,11]
				2065 (solid, 14 °C) [1]
$KF \cdot 2H_2O$	41.4 [7]	n.a.	n.a.	n.a.
$K(CH_3COO) \cdot 1\frac{1}{2}H_2O$	42 [8]	n.a.	n.a.	n.a.
$K_3PO_4 \cdot 7H_2O$	45 [8]	n.a.	n.a.	n.a.
$Zn(NO_3)_2 \cdot 4H_2O$	45.5 [8]	n.a.	n.a.	n.a.
$Ca(NO_3)_2 \cdot 4H_2O$	42.7 [7]	n.a.	n.a.	n.a.
	47 [8]			
$Na_2HPO_4 \cdot 7H_2O$	48 [7]	n.a.	n.a.	n.a.

Table A.1 (Continued): Inorganic substances [25]

Compound	Melting temperature (°C)	Heat of fusion (kJ/kg)	Thermal conductivity (W/m K)	Density (kg/m^3)
$Na_2S_2O_3 \cdot 5H_2O$	48 [1,6–8] 48–49 [12]	201 [1] 209.3 [12] 187 [6]	n.a.	1600 (solid) [1] 1666 [12]
$Zn(NO_3)_2 \cdot 2H_2O$	54 [8]	n.a.	n.a.	n.a.
$NaOH \cdot H_2O$	58.0 [7]	n.a.	n.a.	n.a.
$Na(CH_3COO) \cdot 3H_2O$	58 [6,13] 58.4 [7,14–20]	264 [14–20] 226 [6]	n.a.	1450 [6]
$Cd(NO_3)_2 \cdot 4H_2O$	59.5 [7]	n.a.	n.a.	n.a.
$Fe(NO_3)_2 \cdot 6H_2O$	60 [8]	n.a.	n.a.	n.a.
NaOH	64.3 [6]	227.6 [6]	n.a.	1690 [6]
$Na_2B_4O_7 \cdot 10H_2O$	68.1 [7]	n.a.	n.a.	n.a.
$Na_3PO_4 \cdot 12H_2O$	69 [7]	n.a.	n.a.	n.a.
$Na_2P_2O_7 \cdot 10H_2O$	70 [6]	184 [6]		n.a.
$Ba(OH)_2 \cdot 8H_2O$	78 [1,4,6,7,11,13]	265.7 [4,11]	0.653 (liquid, 85.7 °C) [4,11]	1937 (liquid, 84 °C) [4,11]
		267 [1]	0.678 (liquid, 98.2 °C) [11]	2070 (solid, 24 °C) [4,6,11]
		280 [6]	1.255 (solid, 23 °C) [4,11]	2180 (solid) [1]
$AlK(SO_4)_2 \cdot 12H_2O$	80 [8]	n.a.	n.a.	n.a.
$KaI(SO_4)_2 \cdot 12H_2O$	85.8 [7]	n.a.	n.a.	n.a.
$Al_2(SO_4)_3 \cdot 18H_2O$	88 [7]	n.a.	n.a.	n.a.
$Al(NO_3)_3 \cdot 8H_2O$	89 [8]	n.a.	n.a.	n.a.
$Mg(NO_3)_2 \cdot 6H_2O$	89 [4,6,11]	162.8 [4,11]	0.490 (liquid, 95 °C) [4,11]	1550 (liquid, 94 °C) [4,11]
	90 [7,8]	149.5 [6]	0.502 (liquid, 110 °C) [11]	1636 (solid, 25 °C) [4,11]
			0.611 (solid, 37 °C) [4,11] 0.669 (solid, 55.6 °C) [11]	1640 [6]
$(NH_4)Al(SO_4) \cdot 6H_2O$	95 [6,8]	269 [6]	n.a.	n.a.
$Na_2S \cdot 5\frac{1}{2}H_2O$	97.5 [8]	n.a.	n.a.	n.a.
$CaBr_2 \cdot 4H_2O$	110 [8]	n.a.	n.a.	n.a.
$Al_2(SO_4)_3 \cdot 16H_2O$	112 [8]	n.a.	n.a.	n.a.
$MgCl_2 \cdot 6H_2O$	117 [4,6,7,11]	168.6 [4,11]	0.570 (liquid, 120 °C) [4,11]	1450 (liquid, 120 °C) [4,11]
	115 [8]	165 [1,6]	0.598 (liquid, 140 °C) [11]	1442 (liquid, 78 °C) [1]
	116 [1]		0.694 (solid, 90 °C) [4,11] 0.704 (solid, 110 °C) [11]	1569 (solid, 20 °C) [4,11] 1570 (solid, 20 °C) [1]
$Mg(NO_3) \cdot 2H_2O$	130 [8]	n.a.	n.a.	n.a.
$NaNO_3$	307 [21] 308 [22,23]	172 [21] 174 [23] 199 [22]	0.5 [22]	2260 [21] 2257 [22]
KNO_3	333 [22] 336 [23]	266 [22] 116 [23]	0.5 [23]	2.110 [23]
KOH	380 [22]	149.7 [22]	0.5 [22]	2.044 [22]
$MgCl_2$	714 [21]	452 [21]	n.a.	2140 [21]
NaCl	800 [21] 802 [22]	492 [21] 466.7 [22]	5 [22]	2160 [21,22]

Table A.2: Inorganic eutectic substances [25]

Compound	Melting temperature (°C)	Heat of fusion (kJ/kg)	Thermal conductivity (W/m K)	Density (kg/m³)
66.6% $CaCl_2 \cdot 6H_2O$ + 33.3% $MgCl_2 \cdot 6H_2O$	25 [6]	127 [6]	n.a.	1590 [6]
48% $CaCl_2$ + 4.3% NaCl + 0.4% KCl + 47.3% H_2O	26.8 [1,6]	188.0 [6]	n.a.	1640 [6]
47% $Ca(NO_3)_2 \cdot 4H_2O$ + 33% $Mg(NO_3)_2 \cdot 6H_2O$	30 [1]	136 [1]	n.a.	n.a.
60% $Na(CH_3COO) \cdot 3H_2O$ + 40% $CO(NH_2)_2$	31.5 [24] 30 [25]	226 [24] 200.5 [25]	n.a.	n.a.
61.5% $Mg(NO_3)_2 \cdot 6H_2O$ + 38.5% NH_4NO_3	52 [11]	125.5 [11]	0.494 (liquid, 65.0 °C) [11] 0.515 (liquid, 88.0 °C) [11] 0.552 (solid, 36.0 °C) [11]	1515 (liquid, 65 °C) [11] 1596 (solid, 20 °C) [11]
58.7% $Mg(NO_3) \cdot 6H_2O$ + 41.3% $MgCl_2 \cdot 6H_2O$	59 [11] 58 [6]	132.2 [11] 132 [6]	0.510 (liquid, 65.0 °C) [11] 0.565 (liquid, 85.0 °C) [11] 0.678 (solid, 38.0 °C) [11] 0.678 (solid, 53.0 °C) [11]	1550 (liquid, 50 °C) [11] 1630 (solid, 24 °C) [11]
53% $Mg(NO_3)_2 \cdot 6H_2O$ + 47% $Al(NO_3)_2 \cdot 9H_2O$	61 [1]	148 [1]	n.a.	n.a.
14% $LiNO_3$ + 86% $Mg(NO_3)_2 \cdot 6H_2O$	72 [6]	>180 [6]	n.a.	1590 (liquid) [6] 1610 (solid) [6]
66.6% urea + 33.4% NH_4Br	76 [11]	161.0 [11]	0.331 (liquid, 79.8 °C) [11] 0.324 (liquid, 92.5 °C) [11] 0.649 (solid, 39.0 °C) [11] 0.682 (solid, 65 °C) [11]	1440 (liquid, 85 °C) [11] 1548 (solid, 24 °C) [11]
11.8% NaF + 54.3% KF + 26.6% LiF + 7.3% MgF_2	449 [26]	n.a.	n.a.	2160 (liquid) [26]
35.1% LiF + 38.4% NaF + 26.5% CaF_2	615 [26]	n.a.	n.a.	2225 (liquid) [26] 2820 (solid, 25 °C) [26]
32.5% LiF + 50.5% NaF + 17.0% MgF_2	632 [26]	n.a.	n.a.	2105 (liquid) [26] 2810 (solid, 25 °C) [26]
51.8% NaF + 34.0% CaF_2 + 14.2% MgF_2	645 [26]	n.a.	n.a.	2370 (liquid) [26] 2970 (solid, 25 °C) [26]
48.1% LiF + 51.9% NaF	652 [26]	n.a.	n.a.	1930 (liquid) [26] 2720 (solid, 25 °C) [26]
63.8% KF + 27.9% NaF + 8.3% MgF_2	685 [26]	n.a.	n.a.	2090 (liquid) [26]
45.8% LiF + 54.2% MgF_2	746 [26]	n.a.	n.a.	2305 (liquid) [26] 2880 (solid, 25 °C) [26]
53.6% NaF + 28.6% MgF_2 + 17.8% KF	809 [26]	n.a.	n.a.	2110 (liquid) [26] 2850 (solid, 25 °C) [26]
66.9% NaF + 33.1% MgF_2	832 [26]	n.a.	n.a.	2190 (liquid) [26] 2940 (solid, 25 °C) [26]

Table A.3: Non-eutectic mixtures of inorganic substances [25]

Compound	Melting temperature (°C)	Heat of fusion (kJ/kg)	Thermal conductivity (W/m K)	Density (kg/m³)
H_2O + polyacrylamid	0 [5]	292 [5]	0.486 (30 °C) [5]	1047 (30 °C) [5]
50% $Na(CH_3COO) \cdot 3H_2O$ + 50% $HCONH_2$	40.5 [27]	255 [27]	n.a.	n.a.
$Mg(NO_3)_2 \cdot 6H_2O$/ $Mg(NO_3)_2 \cdot 2H_2O$	55.5 [8]	n.a.	n.a.	n.a.
$KOH \cdot H_2O$/KOH	99 [8]	n.a.	n.a.	
68.1% KCl + 31.9% $ZnCl_2$	235 [21]	198 [21]	n.a.	2480 [21]
38.5% MgCl + 61.5% NaCl	435 [21]	328 [21]	n.a.	2160 [21]
Salt-ceramics $NaCO_3$–$BaCO_3$/MgO	500–850 [22]	415.4 [22]	5 [22]	2.600 [22]

Table A.4: Organic substances [25]

Compound	Melting temperature (°C)	Heat of fusion (kJ/kg)	Thermal conductivity (W/m K)	Density (kg/m^3)
Paraffin C_{14}	4.5 [1]	165 [1]	n.a.	n.a.
Paraffin C_{15}–C_{16}	8 [1]	153 [1]	n.a.	n.a.
Polyglycol E400	8 [4,11]	99.6 [4,11]	0.187 (liquid, 38.6 °C) [4,11] 0.185 (liquid, 69.9 °C) [11]	1125 (liquid, 25 °C) [4,11] 1228 (solid, 3 °C) [4,11]
Dimethyl-sulfoxide (DMS)	16.5 [28]	85.7 [28]	n.a.	1009 (solid and liquid) [28]
Paraffin C_{16}–C_{18}	20–22 [29]	152 [29]	n.a.	n.a.
Polyglycol E600	22 [4,11]	127.2 [4,11]	0.189 (liquid, 38.6 °C) [4,11] 0.187 (liquid, 67.0 °C) [11]	1126 (liquid, 25 °C) [4,11] 1232 (solid, 4 °C) [4,11]
Paraffin C_{13}–C_{24}	22–24 [1]	189 [1]	0.21 (solid) [1]	0.760 (liquid, 70 °C) [1] 0.900 (solid, 20 °C) [1]
1-Dodecanol	26 [9]	200 [9]	n.a.	n.a.
Paraffin C_{18}	28 [1] 27.5 [30]	244 [1] 243.5 [30]	0.148 (liquid, 40 °C) [30] 0.15 (solid) [1] 0.358 (solid, 25 °C) [30]	0.774 (liquid, 70 °C) [1] 0.814 (solid, 20 °C) [1]
1-Tetradecanol	38 [9]	205 [9]		
Paraffin C_{16}–C_{28}	42–44 [1]	189 [1]	0.21 (solid) [1]	0.765 (liquid, 70 °C) [1] 0.910 (solid, 20 °C) [1]
Paraffin C_{20}–C_{33}	48–50 [1]	189 [1]	0.21 (solid) [1]	0.769 (liquid, 70 °C) [1] 0.912 (solid, 20 °C) [1]
Paraffin C_{22}–C_{45}	58–60 [1]	189 [1]	0.21 (solid) [1]	0.795 (liquid, 70 °C) [1] 0.920 (solid, 20 °C) [1]
Parffin wax	64 [4,11]	173.6 [4,11] 266 [6]	0.167 (liquid, 63.5 °C) [4,11] 0.346 (solid, 33.6 °C) [4,11] 0.339 (solid, 45.7 °C) [11]	790 (liquid, 65 °C) [4,11] 916 (solid, 24 °C) [4,11]
Polyglycol E6000	66 [4,11]	190.0 [4,11]	n.a.	1085 (liquid, 70 °C) [4,11] 1212 (solid, 25 °C) [4,11]
Paraffin C_{21}–C_{50}	66–68 [1]	189 [1]	0.21 (solid) [1]	0.830 (liquid, 70 °C) [1] 0.930 (solid, 20 °C) [1]
Biphenyl	71 [4,11]	119.2 [4,11]	n.a.	991 (liquid, 73 °C) [4,11] 1166 (solid, 24 °C) [11]
Propionamide	79 [11]	168.2 [11]	n.a.	n.a.
Naphthalene	80 [4,11]	147.7 [4,11]	0.132 (liquid, 83.8 °C) [4,11] 0.341 (solid, 49.9 °C) [4,11] 0.310 (solid, 66.6 °C) [11]	976 (liquid, 84 °C) [4,11] 1145 (solid, 20 °C) [4,11]
Erythritol	118.0 [31]	339.8 [31]	0.326 (liquid, 140 °C) [31] 0.733 (solid, 20 °C) [31]	1300 (liquid, 140 °C) [31] 1480 (solid, 20 °C) [31]
HDPE	100–150 [32]	200 [32]	n.a.	n.a.
Trans-1,4-polybutadiene (TPB)	145 [33]	144 [33]	n.a.	n.a.

Table A.5: Organic eutectic substances [25]

Compound	Melting temperature (°C)	Heat of fusion (kJ/kg)	Thermal conductivity (W/m K)	Density (kg/m^3)
37.5% Urea + 63.5% acetamide	53 [1]	n.a.	n.a.	n.a.
67.1% Naphthalene + 32.9% benzoic acid	67 [11]	123.4 [11]	0.136 (liquid, 78.5 °C) [11] 0.130 (liquid, 100 °C) [11] 0.282 (solid, 38 °C) [11] 0.257 (solid, 52 °C) [11]	n.a.

Table A.6: Fatty acid substances [25]

Compound	Melting temperature (°C)	Heat of fusion (kJ/kg)	Thermal conductivity (W/m K)	Density (kg/m^3)
Propyl palmiate	10 [9]	186 [9]	n.a.	n.a.
Isopropyl palmiate	11 [34]	95–100 [34]	n.a.	n.a.
Capric–lauric acid + pentadecane (90:10)	13.3 [35]	142.2 [35]	n.a.	n.a.
Isopropyl stearate	14–18 [34]	140–142 [34]	n.a.	n.a.
Caprylic acid	16 [4,11]	148.5 [4,11]	0.149 (liquid, 38.6 °C) [4,11]	901 (liquid, 30 °C) [4,11]
	16.3 [1]	149 [1]	0.145 (liquid, 67.7 °C) [11] 0.148 (liquid, 20 °C) [1]	862 (liquid, 80 °C) [1] 981 (solid, 13 °C) [4,11] 1033 (solid, 10 °C) [1]
Capric–lauric acid (65 mol%–35 mol%)	18.0 [36]	148 [36]	n.a.	n.a.
Butyl stearate	19 [9]	140 [9] 123–200 [34]	n.a.	n.a.
Capric–lauric acid (45–55%)	21 [9]	143 [9]	n.a.	n.a.
Dimethyl sabacate	21 [34]	120–135 [34]	n.a.	n.a.
34% Mistiric acid + 66% Capric acid	24 [11]	147.7 [11]	0.164 (liquid, 39.1 °C) [11] 0.154 (liquid, 61.2 °C) [11]	888 (liquid, 25 °C) [11] 1018 (solid, 1 °C) [11]
Vinyl stearate	27–29 [34]	122 [34]	n.a.	n.a.
Capric acid	32 [4,11]	152.7 [4,11]	0.153 (liquid, 38.5 °C) [4,11]	878 (liquid, 45 °C) [4,11]
	31.5 [1]	153 [1]	0.152 (liquid, 55.5 °C) [11] 0.149 (liquid, 40 °C) [1]	886 (liquid, 40 °C) [1] 1004 (solid, 24 °C) [4,11]
Methyl-12 hydroxy-stearate	42–43 [34]	120–126 [34]	n.a.	n.a.
Lauric acid	42–44 [1]	178 [1]	0.147(liquid, 50 °C) [1]	862 (liquid, 60 °C) [11]
	44 [11]	177.4 [11]		870 (liquid, 50 °C) [1] 1007 (solid, 24 °C) [11]
Myristic acid	49–51 [37]	204.5 [37]	n.a.	861 (liquid, 55 °C) [11]
	54 [1]	187 [1]		844 (liquid, 80 °C) [1]
	58 [11]	186.6 [11]		990 (solid, 24 °C) [11]
Palmitic acid	64 [4,11]	185.4 [4,11]	0.162 (liquid, 68.4 °C) [4,11]	850 (liquid, 65 °C) [4,11]
	61 [38,39]	203.4 [38,39]	0.159 (liquid, 80.1 °C) [11]	847 (liquid, 80 °C) [1]
	63 [1]	187 [1]	0.165 (liquid, 80 °C) [1]	989 (solid, 24 °C) [4,11]
Stearic acid	69 [4,11]	202.5 [4,11]	0.172 (liquid, 70 °C) [1]	848 (liquid, 70 °C) [4,11]
	60–61 [39,40]	186.5 [39,40]		965 (solid, 24 °C) [4,11]
	70 [1]	203 [1]		

Table A.7: Commercial PCMs available on the market [25]

PCM name	Type of product	Melting temperature (°C)	Heat of fusion (kJ/kg)	Density (kg/m^3)	Source
SN33	Salt solution	−33	245	1.24	Cristopia [41]
TH-31	n.a.	−31	131	n.a.	TEAP [42]
SN29	Salt solution	−29	233	1.15	Cristopia [41]
SN26	Salt solution	−26	268	1.21	Cristopia [41]
TH-21	n.a.	−21	222	n.a.	TEAP [42]
SN21	Salt solution	−21	240	1.12	Cristopia [41]
STL-21	Salt solution	−21	240	1.12	Mitsubishi Chemical [43]
SN18	Salt solution	−18	268	1.21	Cristopia [41]
TH-16	n.a.	−16	289	n.a.	TEAP [42]
STL-16	n.a.	−16	n.a.	n.a.	Mitsubishi Chemical [43]
SN15	Salt solution	−15	311	1.02	Cristopia [41]
SN12	Salt solution	−12	306	1.06	Cristopia [41]
STLN10	Salt solution	−11	271	1.05	Mitsubishi Chemical [43]
SN10	Salt solution	−11	310	1.11	Cristopia [41]
TH-10	n.a.	−10	283	n.a.	TEAP [42]
STL-6	Salt solution	−6	284	1.07	Mitsubishi Chemical [43]
SN06	Salt solution	−6	284	1.07	Cristopia [41]
TH-4	n.a.	−4	286	n.a.	TEAP [42]
STL-3	Saltsolution	−3	328	1.01	Mitsubishi Chemical [43]
SN03	Saltsolution	−3	328	1.01	Cristopia [41]
ClimSel C 7	n.a.	7	130	n.a.	Climator [44]
RT5	Paraffin	9	205	n.a.	Rubitherm GmbH [45]
ClimSel C 15	n.a.	15	130	n.a.	Climator [44]
ClimSel C 23	Salt hydrate	23	148	1.48	Climator [44]
RT25	Paraffin	26	232		Rubitherm GmbH [45]
STL27	Salt hydrate	27	213	1.09	Mitsubishi Chemical [43]
S27	Salt hydrate	27	207	1.47	Cristopia [41]
RT30	Paraffin	28	206	n.a.	Rubitherm GmbH [45]
TH29	Salt hydrate	29	188	n.a.	TEAP [42]
ClimSel C 32	Salt hydrate	32	212	1.45	Climator [44]
RT40	Paraffin	43	181	n.a.	Rubitherm GmbH [45]
STL47	Salt hydrate	47	221	1.34	Mitsubishi Chemical [43]
ClimSel C 48	n.a.	48	227	1.36	Climator [44]
STL52	Salt hydrate	52	201	1.3	Mitsubishi Chemical [43]
RT50	Paraffin	54	195	n.a.	Rubitherm GmbH [45]
STL55	Salt hydrate	55	242	1.29	Mitsubishi Chemical [43]
TH58	n.a.	58	226	n.a.	TEAP [42]
ClimSel C 58	n.a.	58	259	1.46	Climator [44]
RT65	Paraffin	64	207		Rubitherm GmbH [45]
ClimSel C 70	n.a.	70	194	1.7	Climator [44]
PCM72	Salt hydrate	72	n.a.	n.a.	Merck KgaA [6]

APPENDIX B

DIFFERENTIAL SCANNING CALORIMETRY THERMOGRAMS

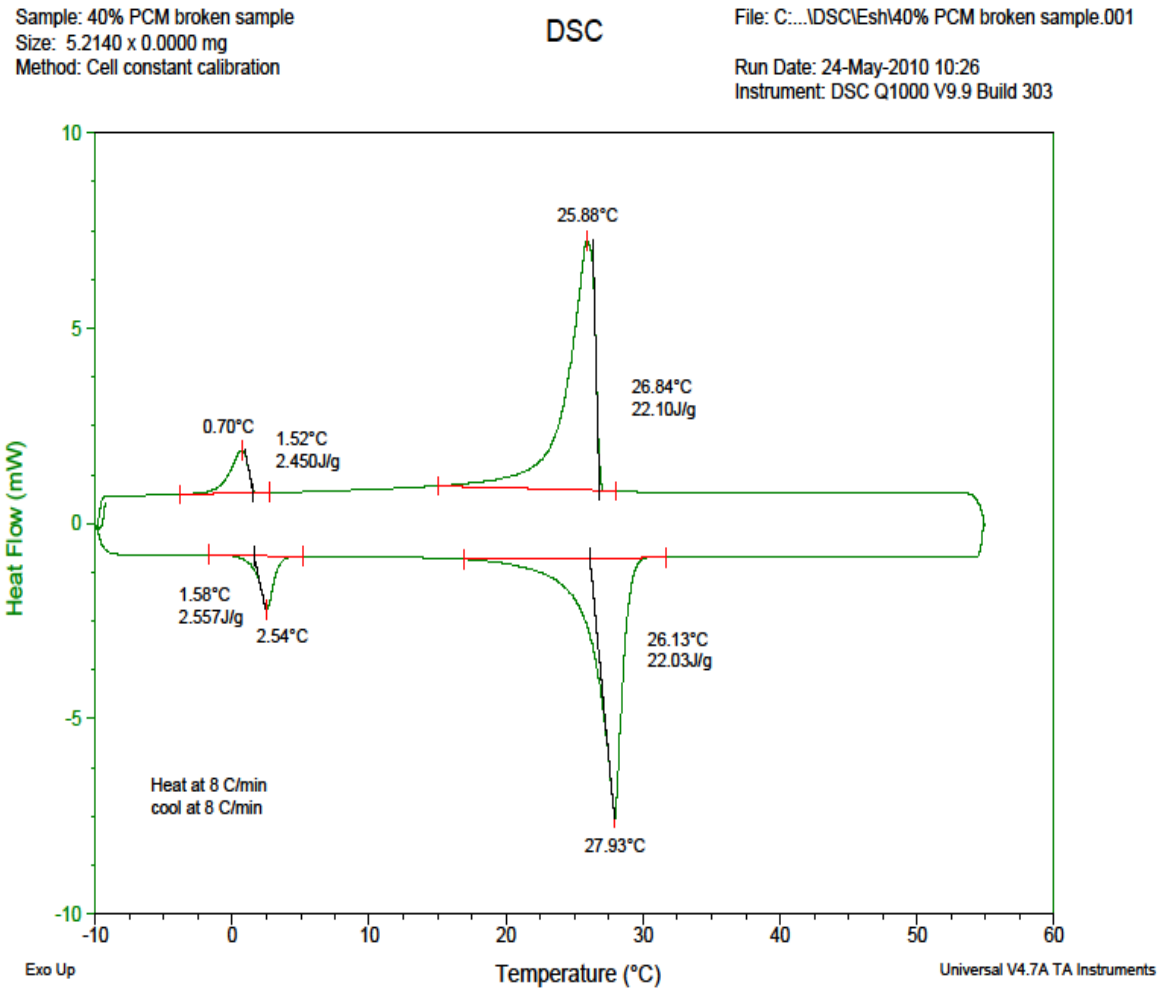

Figure B.1: DSC Curve for 40%MPCM-28D Sample @ 8°C/ min

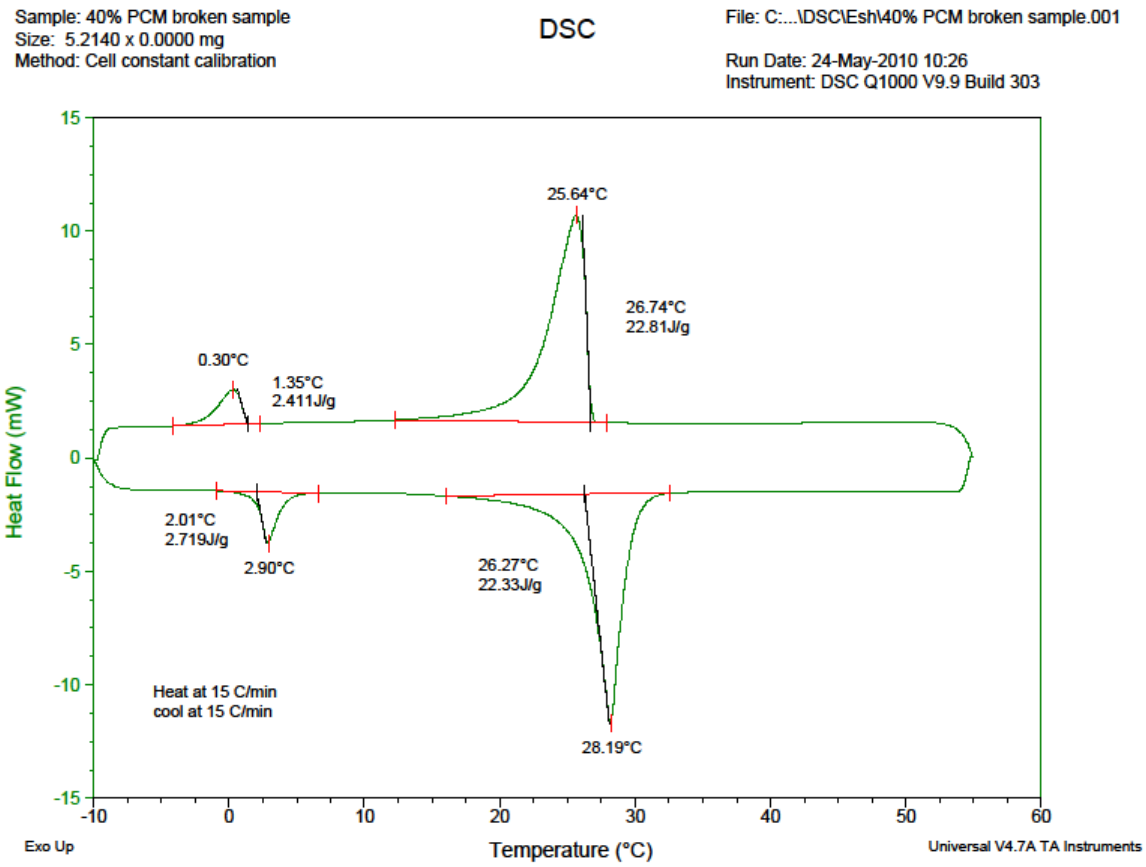

Figure B.2 DSC Curve for 40%MPCM-28D Sample @ 15°C/ min

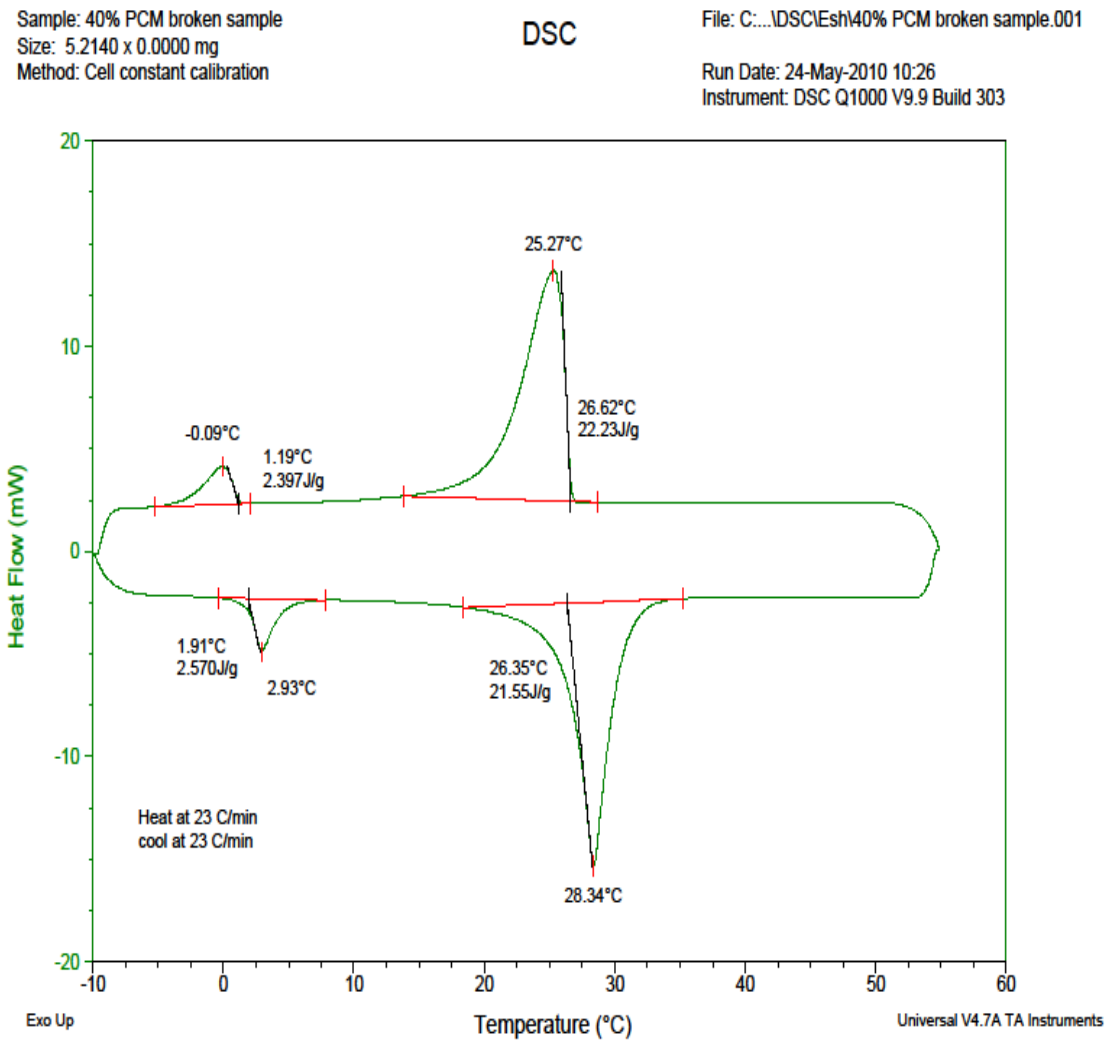

Figure B.3: DSC Curve for 40%MPCM-28D Sample @ 23°C/ min

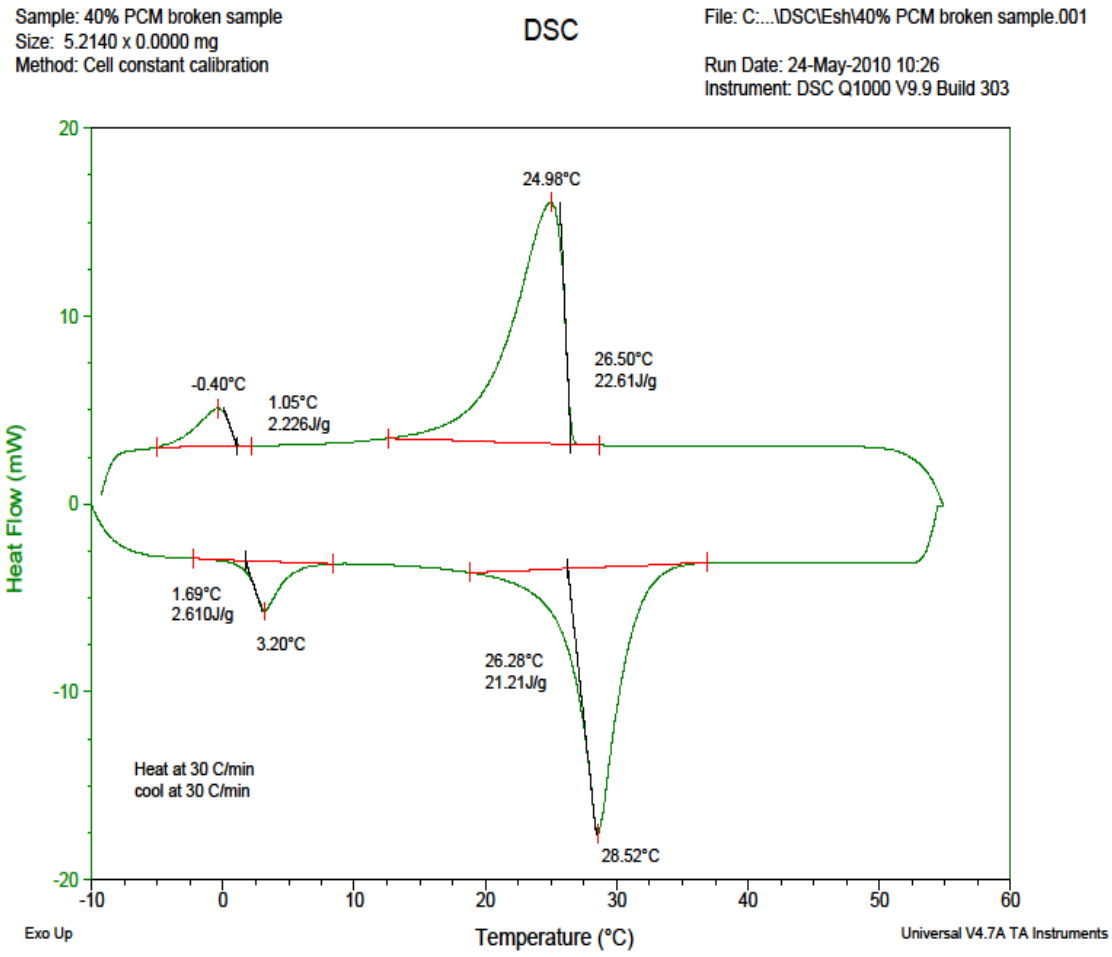

Figure B.4: DSC Curve for 40%MPCM-28D Sample @ 30°C/ min

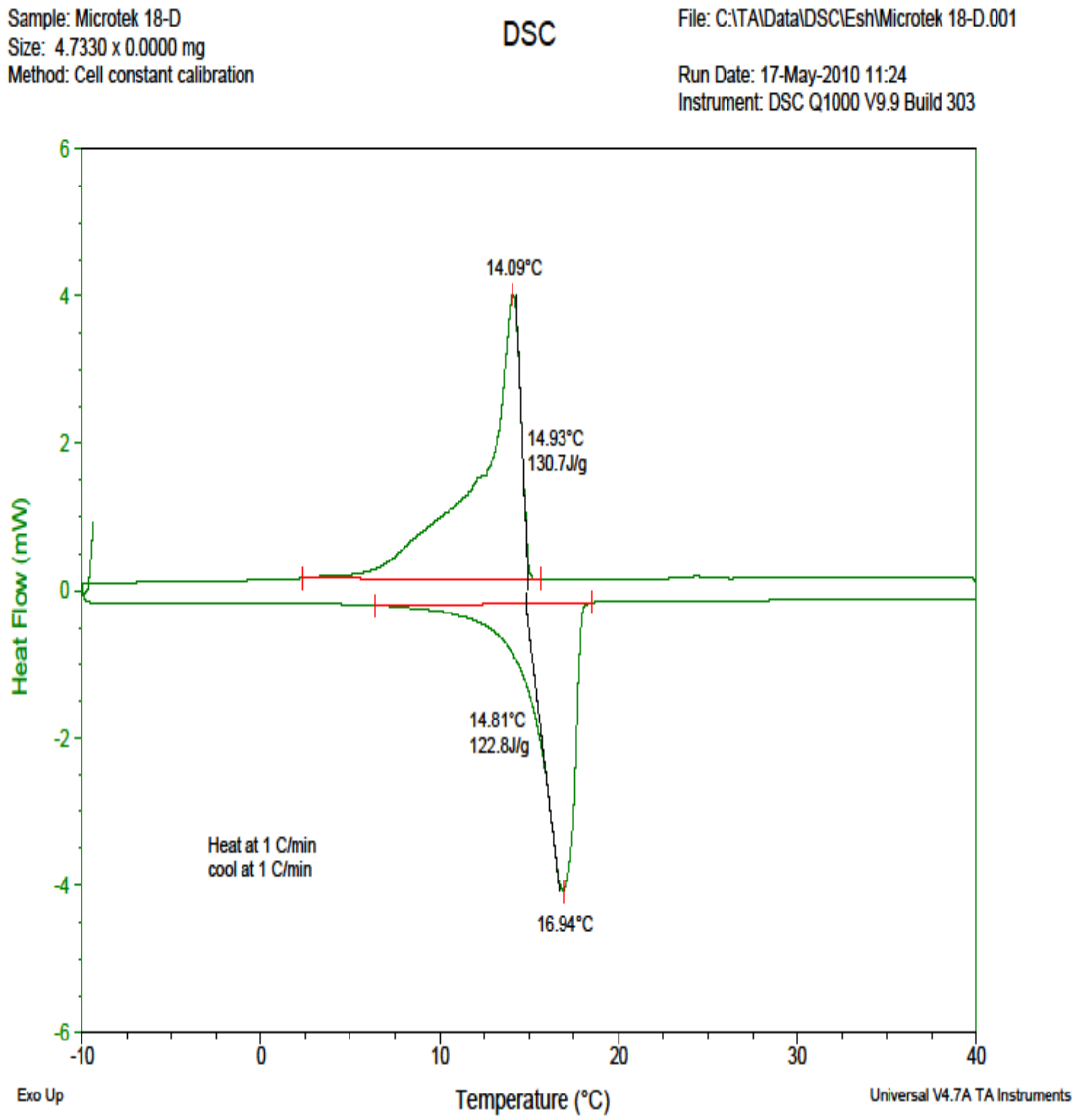

Figure B.5: DSC Curve for pure Microtek MPCM-18D @ 1°C/ min

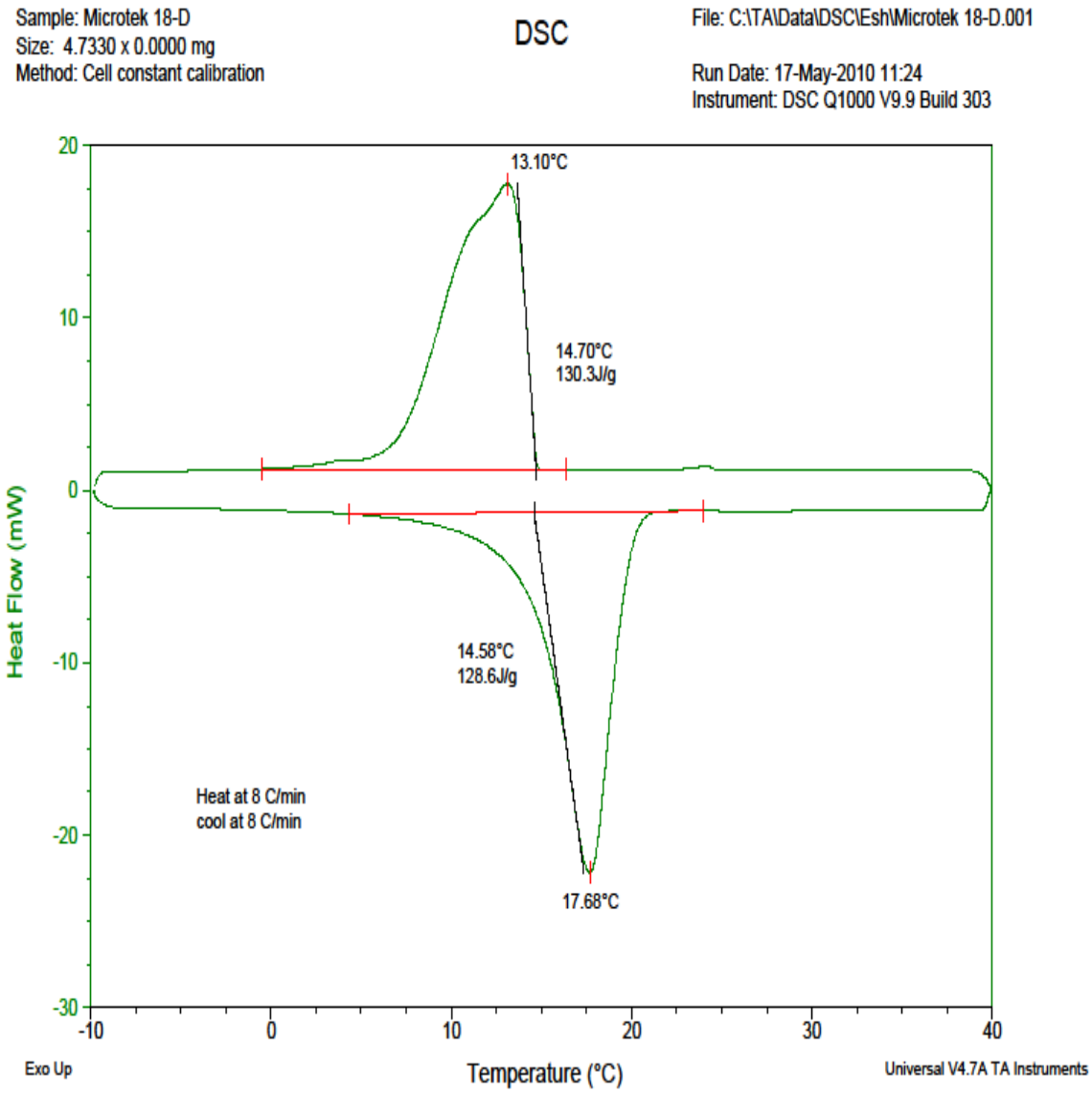

Figure B.6: DSC Curve for pure Microtek MPCM-18D @ 8°C/ min

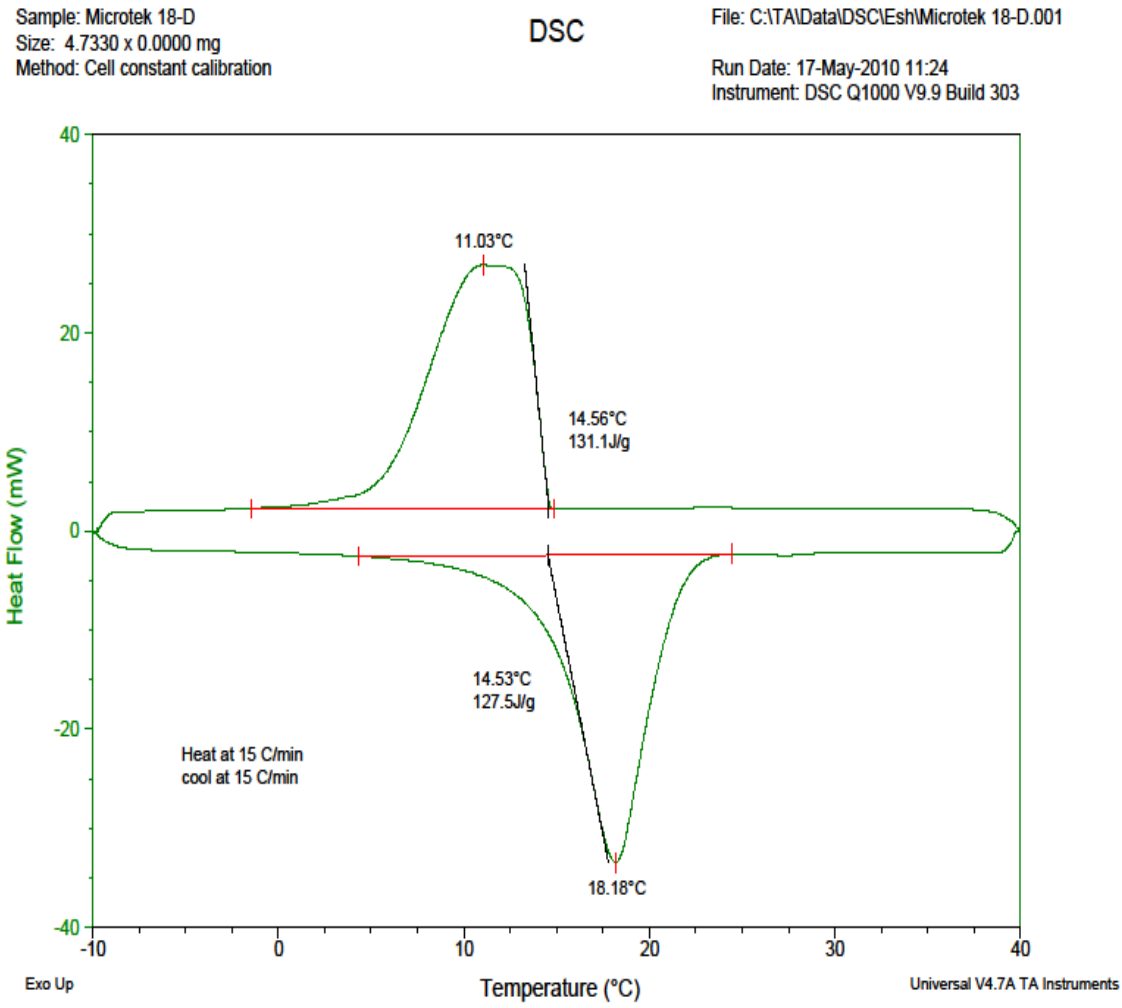

Figure B.7: DSC Curve for pure Microtek MPCM-18D @ 15°C/ min

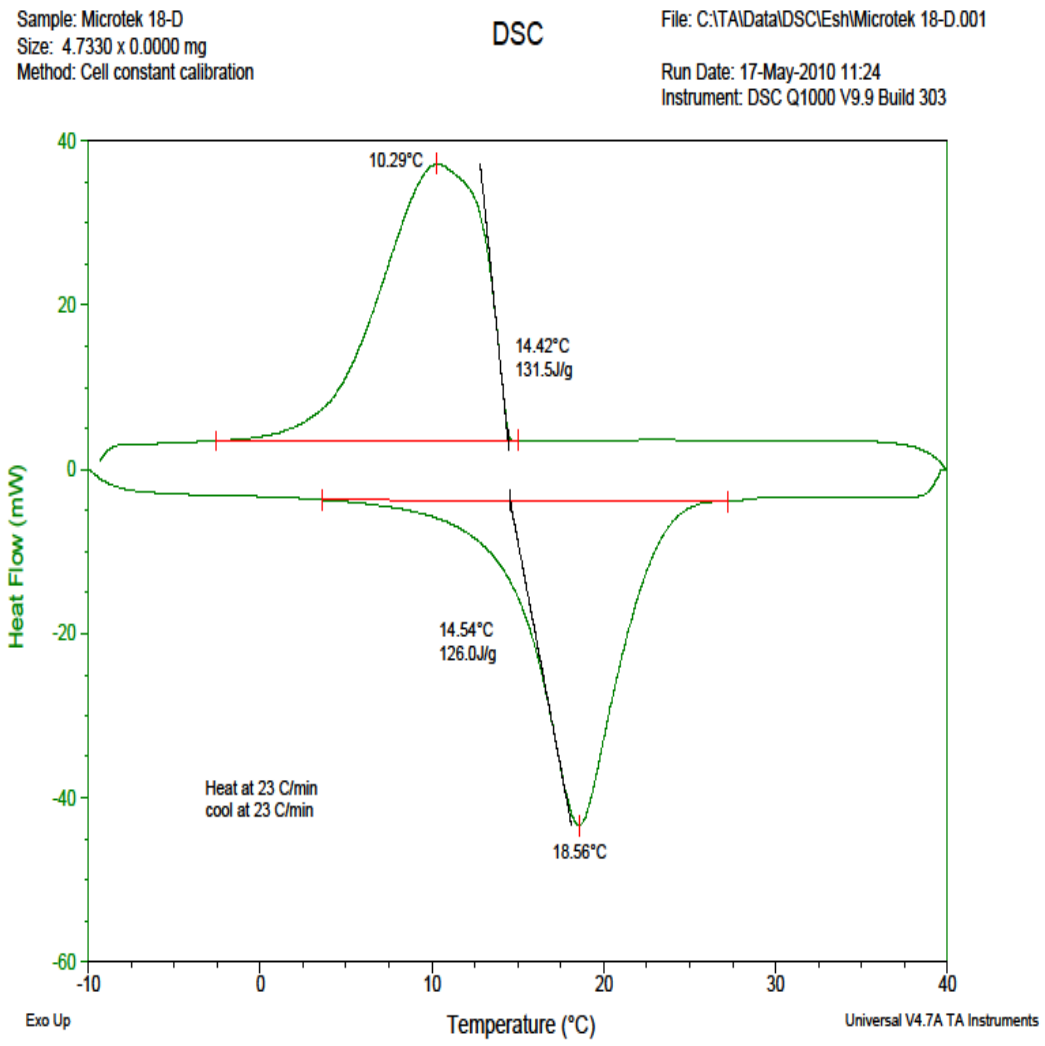

Figure B.8: DSC Curve for pure Microtek MPCM-18D @ 23°C/ min

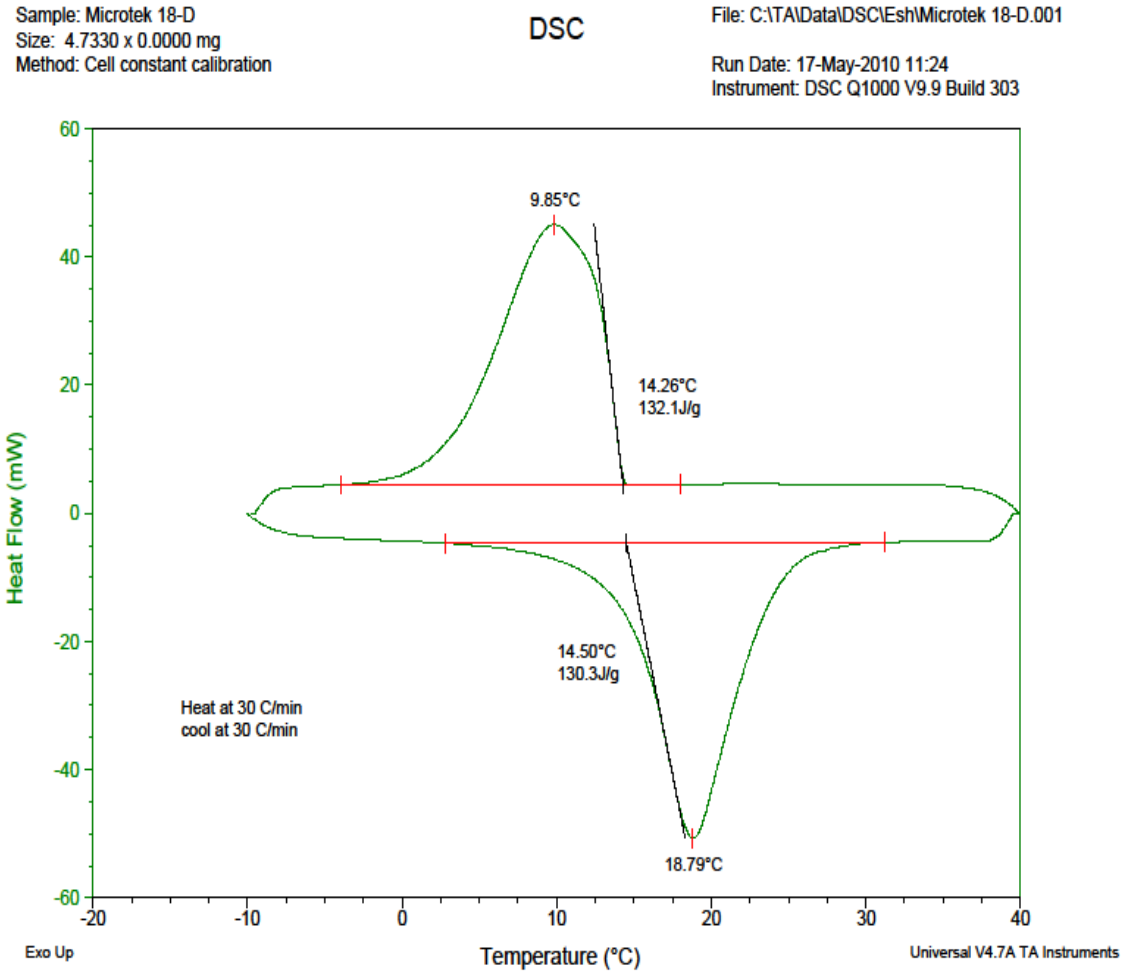

Figure B.9: DSC Curve for pure Microtek MPCM-18D @ 30°C/ min

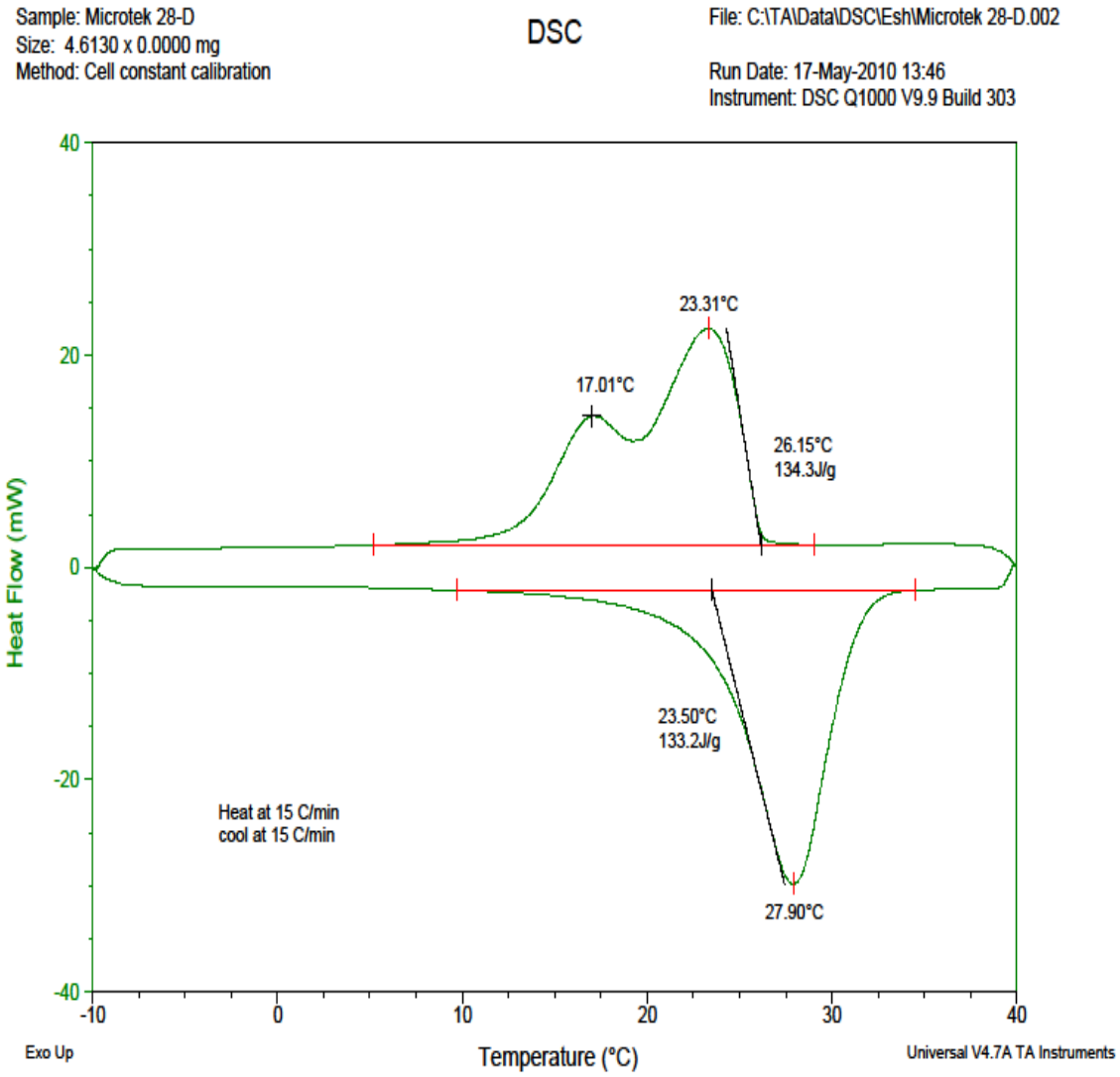

Figure B.10: DSC Curve for pure Microtek MPCM-28D Sample @ 15°C/ min

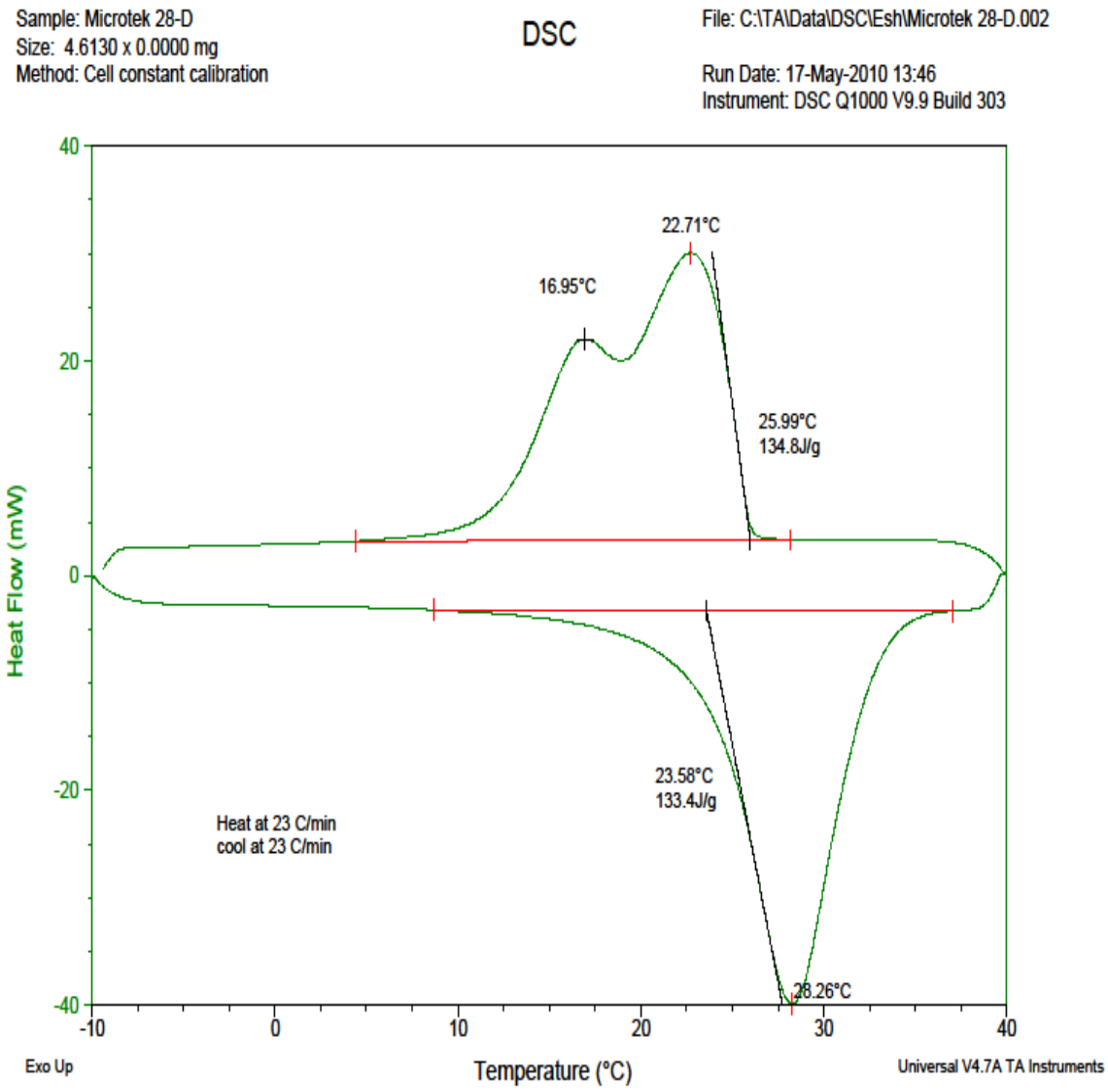

Figure B.11: DSC Curve for pure Microtek MPCM-28D Sample @ 23°C/ min

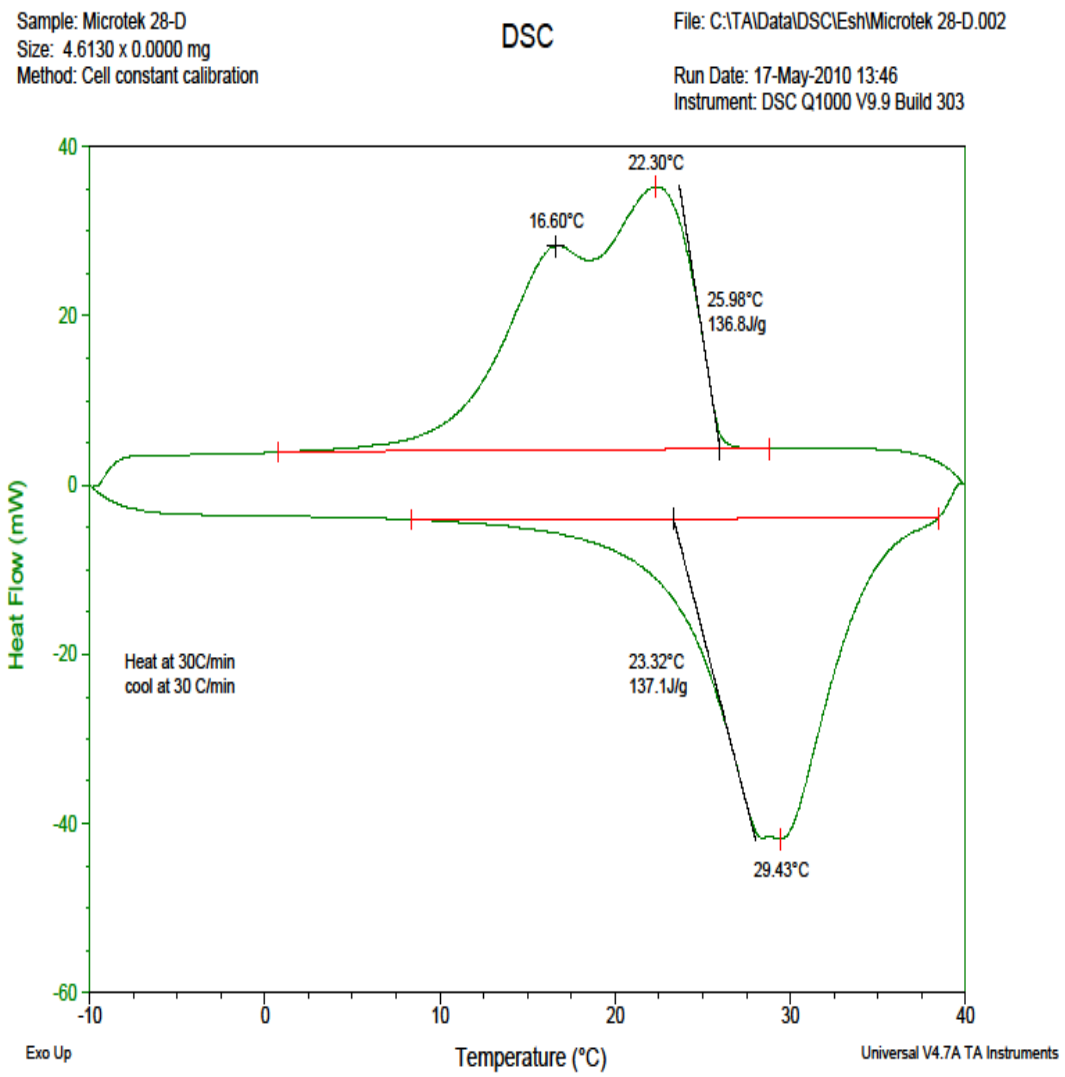

Figure B.12: **DSC curves for pure Microtek MPCM-28D sample at 30°C/ min**

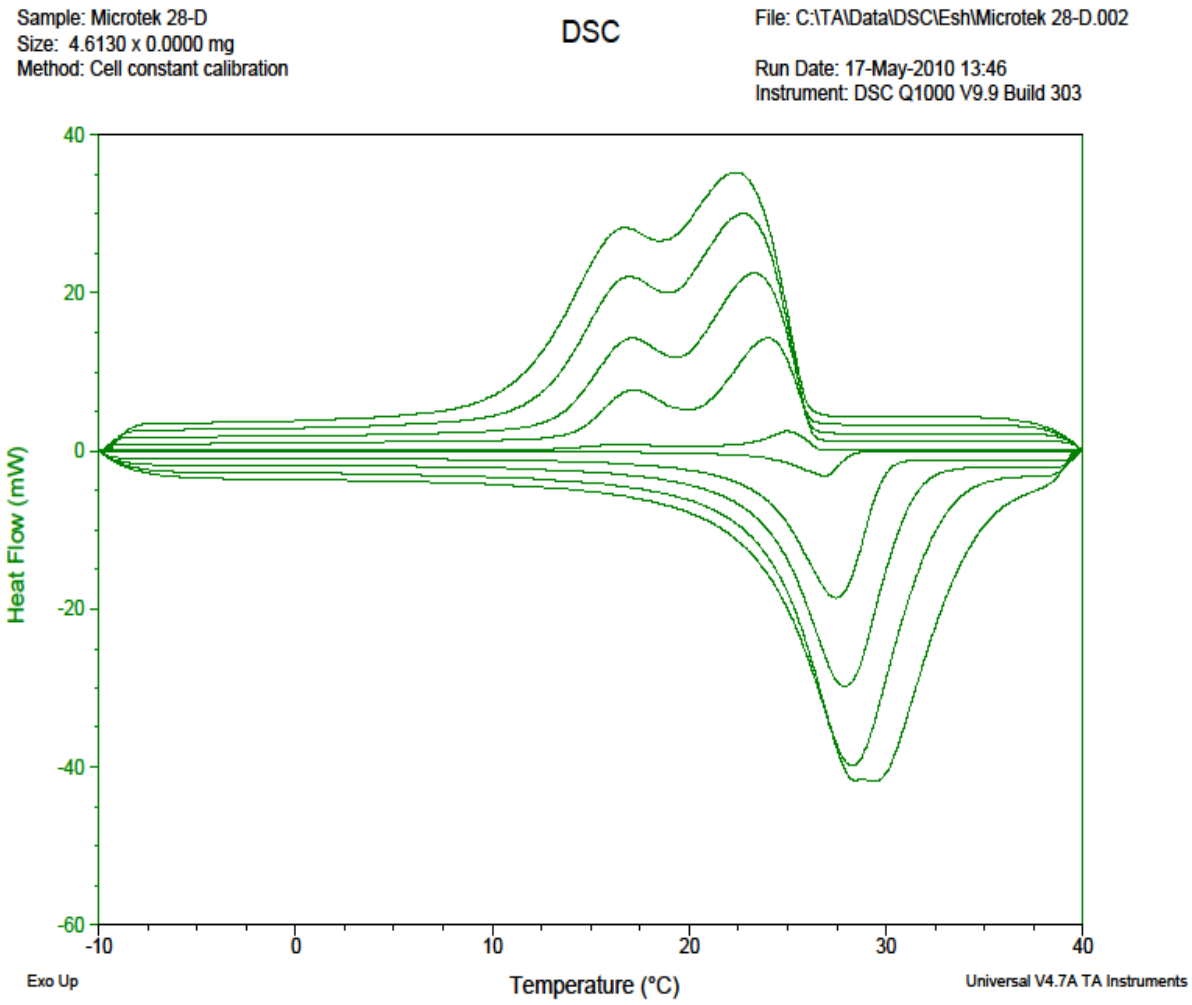

Figure B.13: DSC Curve for Microtek MPCM-28D at all heating rates

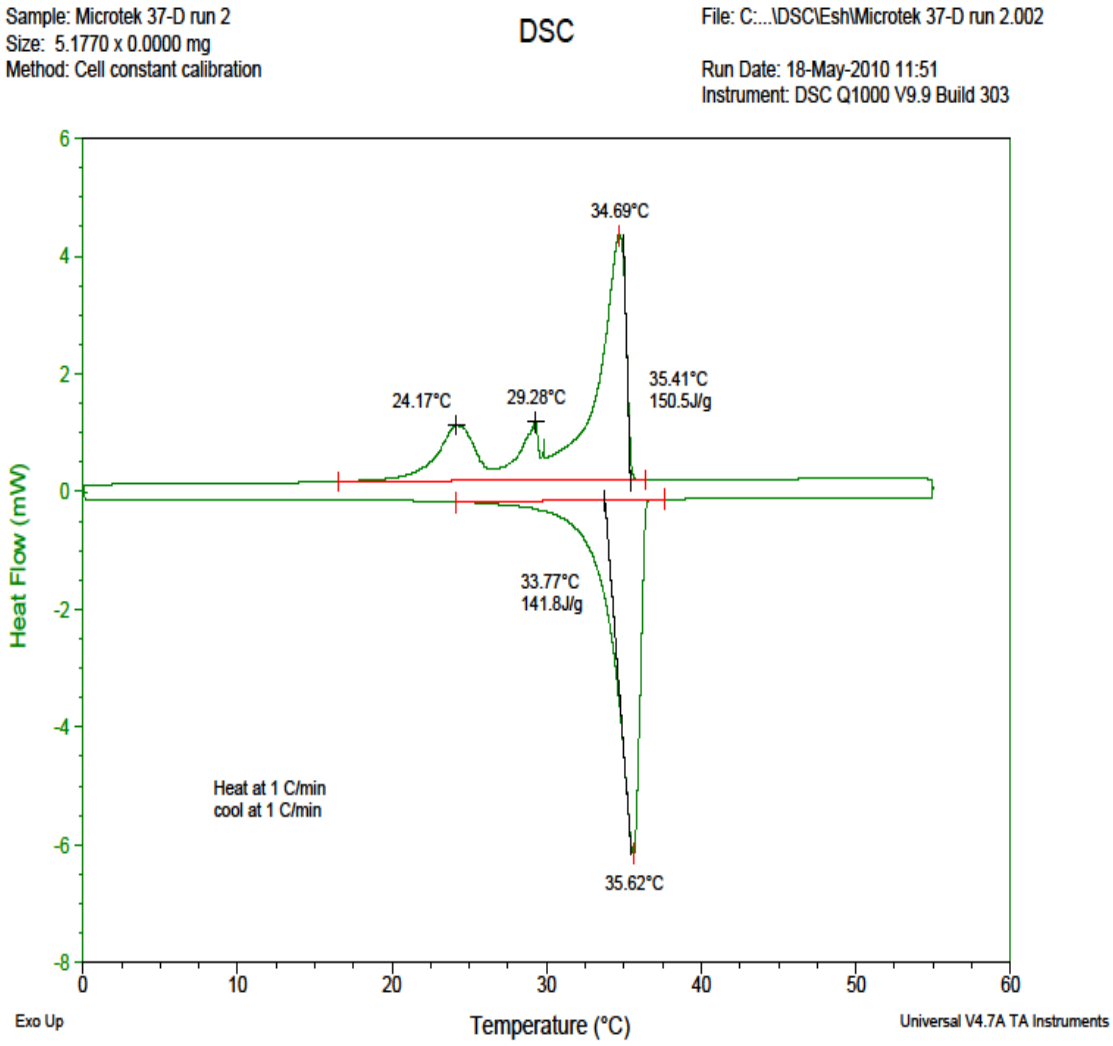

Figure 3.4: DSC Curve for pure Microtek MPCM-37D @ 1°C/min

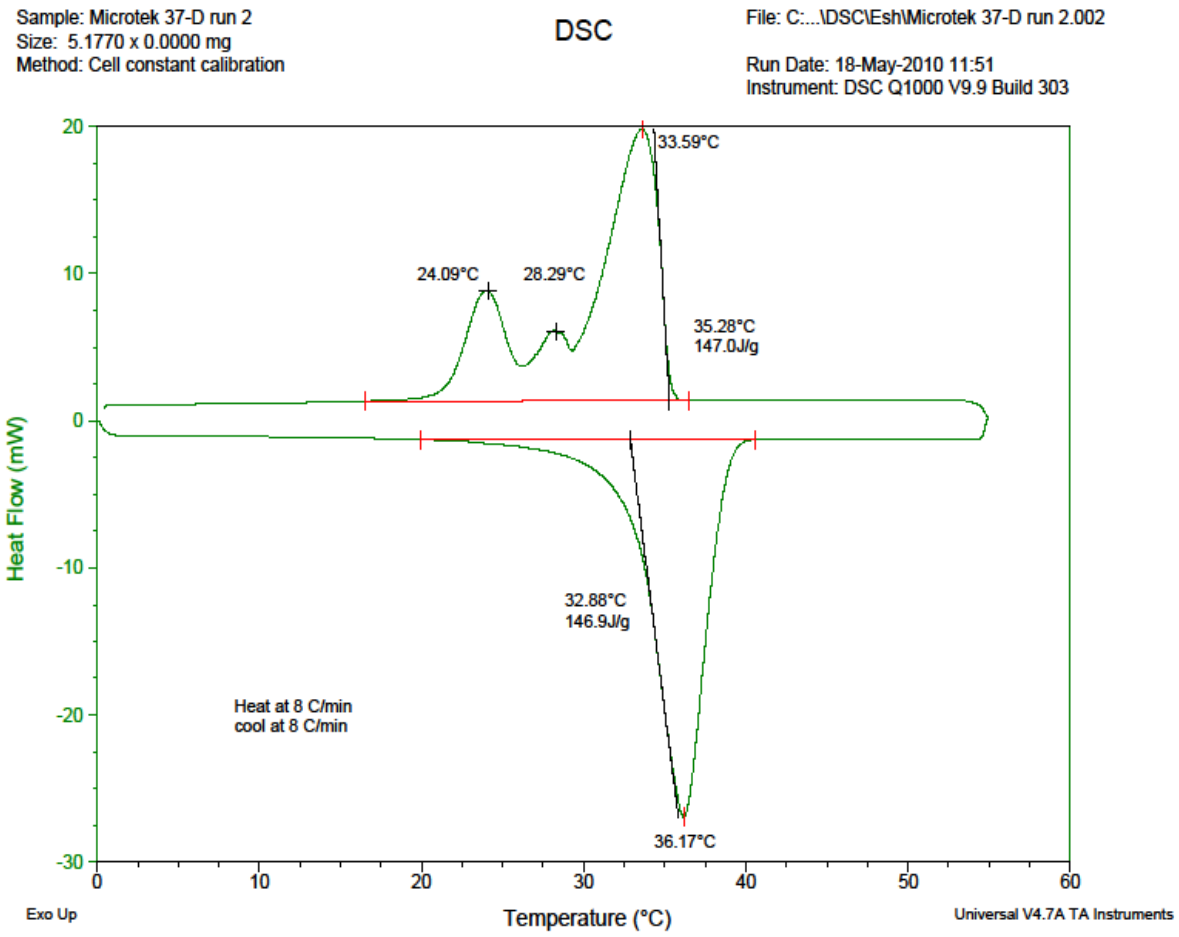

Figure B.14: DSC Curve for pure Microtek MPCM-37D @ 8°C/min

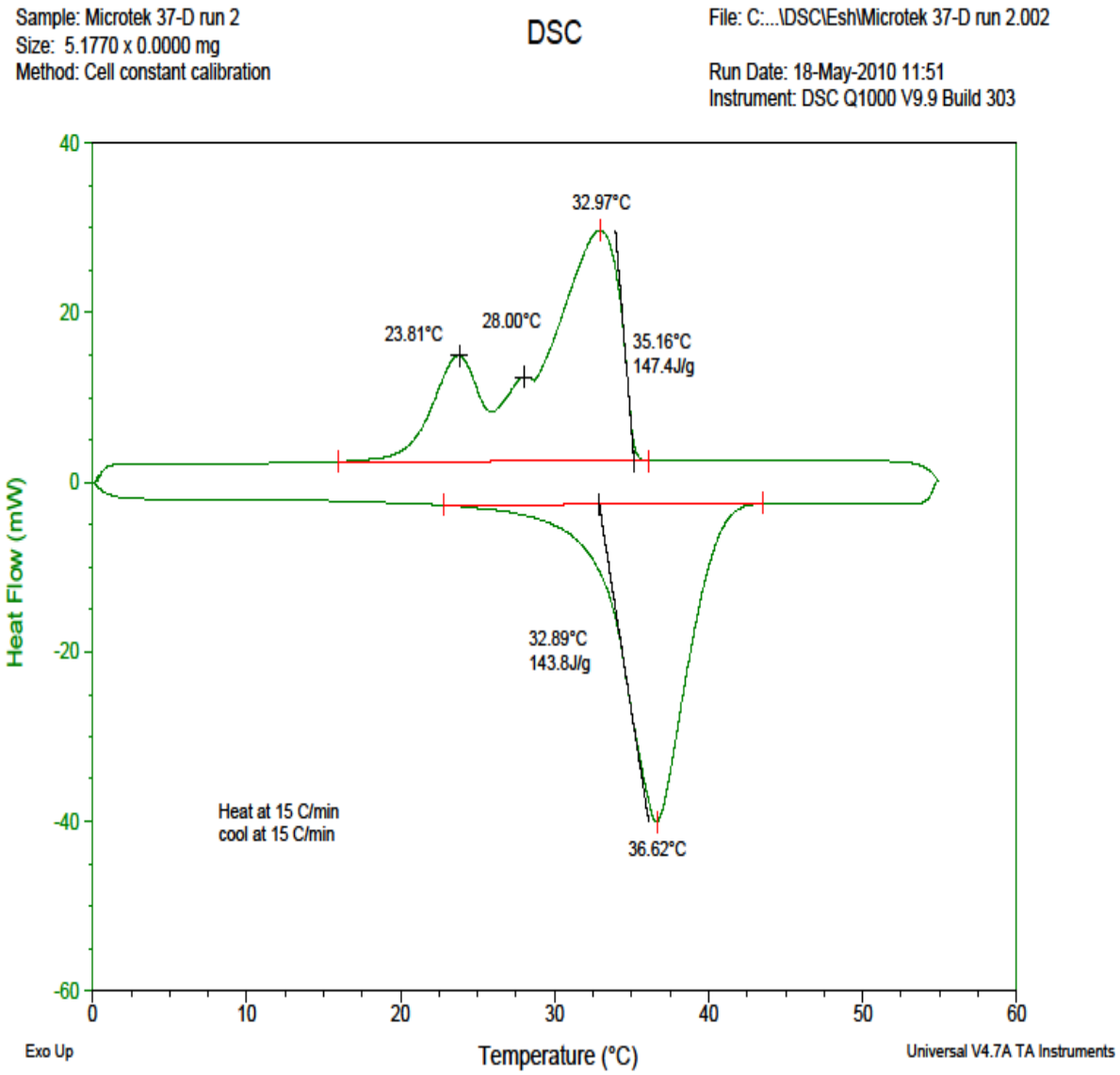

Figure B.15: DSC Curve for pure Microtek MPCM-37D @ 15°C/min

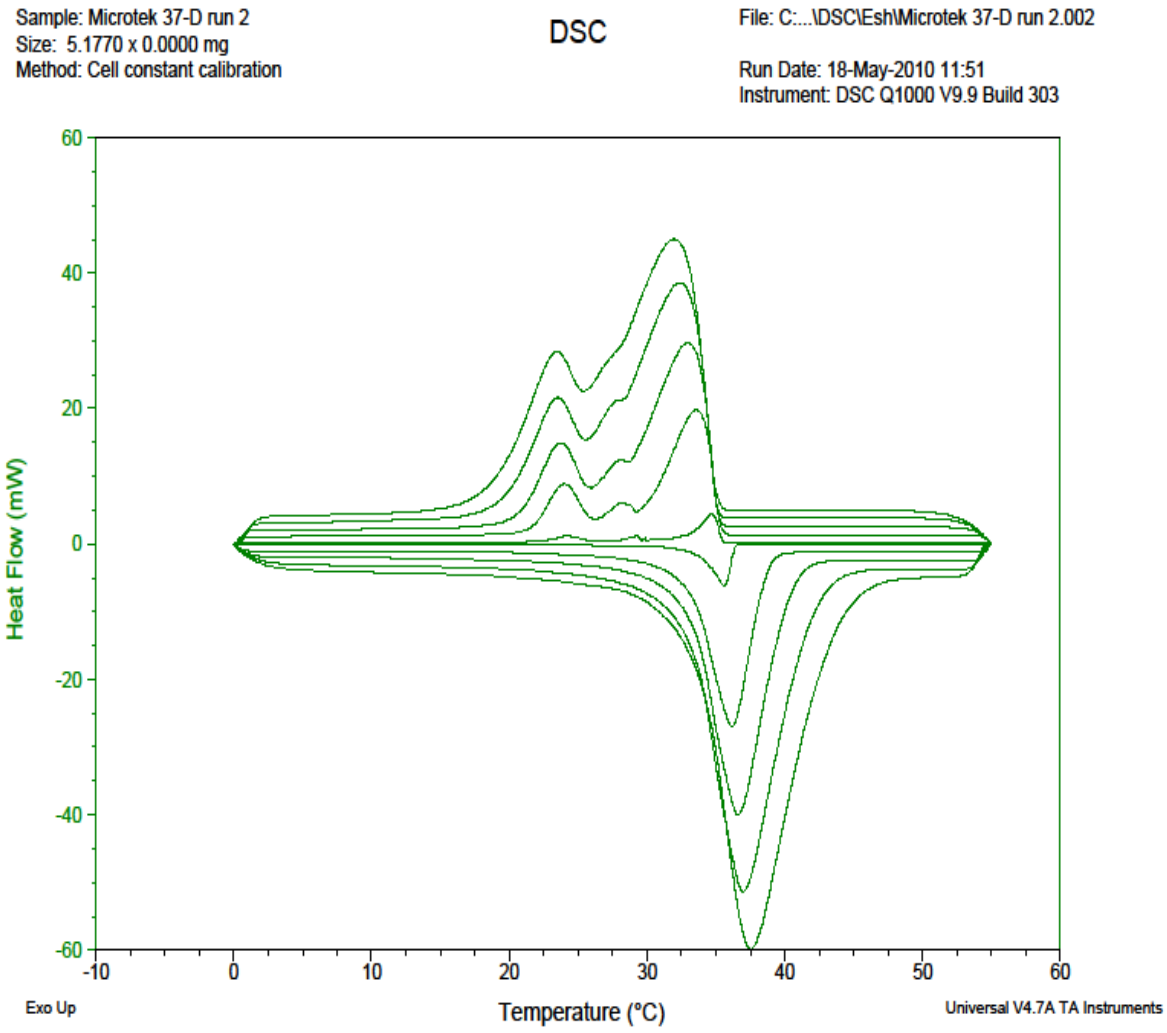

Figure B.16: DSC Curve for pure Microtek MPCM-37D at all heating rates

REFERENCES

[1] Parameshwaran R., Harikrishnan S., Kalaiselvam S., "Energy efficient PCM based variable air volume air conditioning system for modern buildings," *Energy and Buildings*, Vol. 15, Issue 2, 2010.

[2] Stritih U., "An Experimental Model of Thermal Storage System for active heating or cooling of buildings," Internet workshop: http://www.fskab.com/Annex17/ accessed on July 15th, 2010.

[3] Jegadeeshwaran S., Pohekar S., "A Performance enhancement in latent heat thermal storage system," *Renewable and Sustainable Energy Reviews*, Vol. 13, Issue 9, pp. 2225-2244.

[4] Lane G., "Solar Heat Storage: Latent heat materials," *Background and Scientific Principles*, Vol. I, CRC Press, Florida, 1983.

[5] Telkes M., "Thermal storage for solar heating and cooling", *Proceedings of the Workshop on Solar Energy storage Subsystems for the Heating and Cooling of Buildings*, Charlottesville, VA, USA, 1975,

[6] Bordeau L. E.,"Study of two passive solar systems containing phase-change material for thermal storage", *Proceedings of the 5th National Passive Solar Conference*, 1980.

[7] Zalba B., *Free-cooling, an application of PCMs in TES*, Ph.D. Thesis, University of Zaragoza, Spain, 2002.

[8] Vakilaltojjar S. M., Saman W., "Analysis and modeling of a phase change storage system for air conditioning applications", *Appl. Thermal Engineering*, 21, pp. 249-263, 2001.

[9] Vakilaltojjar S. M., Saman W., "Domestic heating and cooling with thermal storage," *Proceedings of Terrastock*, Stuttgart, Germany, 2000.

[10] Bruno F., Saman W., "Testing of a PCM energy storage system for space heating," *Proceedings of the World Renewable Energy Congress VII*, Cologne, Germany, 2002.

[11] Farid M. M., Khudair A.M, Razack S., Al-Hallaj A. K., "A review on phase change energy storage: Materials and applications," *Energy Conversion and Management*, 45, pp. 1597-1615, 2004.

[12] Abhat A, "Low temperature latent heat thermal energy storage. Heat Storage materials," *Solar energy*, 30, pp. 313-32, 1983.

[13] Yinping Zhang, Jianhong Ding, Xin Wang, Rui Yang, Kunping Lin, “Influence of additives on thermal conductivity of shape stabilized phase change material,” *Solar Energy Materials and Solar Cells*, 90, pp. 1692-1702, 2006.

[14] Kuznik F, Virgone J, Lepers S, “Full Scale Experimental Investigation of Room Wall Containing Phase Change Materials Wallboard,” *Proceedings of Climate Well Being Indoors*, 2007.

[15] Banu D, Feldman D, Haghighat F, Paris J, Hawes D., “Energy storing wallboard: Flammability tests,” *Journal of Materials and Civil Engineering*, 10, pp. 98-105, 1998.

[16] YE Hong, Ge Xin-shi, “Preparation of polyethylene paraffin compound as a form stable solid-liquid phase change material,” *Solar Energy Material and Solar Cells*, 64, pp. 37-44, 2000.

[17] Peippo K, Kauranen P, Lund PD, “A multicomponent PCM wall optimized for passive solar heating,” *Energy Building*, ASME, 17, pp. 259-70.

[18] Feustel HE, Steitu C, “Thermal performance of phase change wallboard for residential cooling application,” Lawrence Berkeley National Laboratory, Report LBL-38320, 1997.

[19] Feldman D, Banu D., “Obtaining an energy storing building material by direct incorporation of an organic phase change material in gypsum wall board,” *Solar Energy Materials*, 22, pp. 231-42, 1991.

[20] Kedl RJ, Stovall TK, “Activities in support of the wax impregnated wall board concept,” US Department of Energy thermal Energy storage researchers activity review, 1989.

[21] Fraunhofer, ISE, URL: http://www.ise.fhgde/english, 2002.

[22] Athenitis AK, Liu C, Hawes D, Banu D, Feldman D., “Investigation of the Thermal performance of a passive solar test room with wall latent heat storage,” *Build Environ.*, 32, pp. 405-10, 1997.

[23] Kissock J K, Hannig J M, Whitney T I, Drake M L, “Testing and simulation of phase change wallboard for thermal storage in buildings,” *Proceedings of the 1998 International Solar Energy Conference*, New York, USA, 1998.

[24] Hasnain S.M., “Review on sustainable thermal energy storage technologies, Part 1: Heat storage materials and techniques,” *Energy Conversion Management*, 39 (11), pp. 1127-38, 1998.

[25] Zalba, Belen, Marin Jose.M., Cabeza., Luisa.F.,Mehling Harald., "Review of thermal energy storage with phase change: Materials, Heat transfer analysis and applications," *Applied Thermal Engineering*, 23, 2003.

[26] Gibbs B, Hasnain S., "DSC Study of technical grade phase change heat storage materials for solar heating applications," *Proceedings of the 1995 ASME/JSEJ International Solar Energy Conference, Part 2*, 1995.

[27] Khudair M.Amar , Farid M.Mohd., "A review on energy conservation in building applications with thermal storage by latent heat among phase change materials", *Energy conversion and management*, Vol. 45, Issue 2, Pages 263-275, 2004.

[28] Paris J, Falardeau M, Villeneuve C, "Thermal storage by latent heat: a viable option for energy conservation in buildings," *Energy Sources*, 15, 85-93, 1993.

[29] Pasupathy.A, Velraj.R, Seeniraj R.V, "Phase change material–based building architecture for thermal management in residential and commercial establishments," *Renewable and Sustainable Energy Reviews*, pp. 39-64, 2008.

[30] Farid MM., "A review on energy storage with phase change materials," *Proceedings of Chicago / Midwest Renewable Energy Workshop*, Chicago, USA, 2001.

[31] Murat Kenisarin, Khamid Mahkamov, "Solar Energy Storage using Phase change materials –Science Direct," *Renewable and Sustainable Energy Reviews*, 11, pp. 1913-1965, 1997.

[32] Salyer IO, Sircar AK, Chartoff RP, Miller DE, "Advanced phase change materials for passive solar storage applications," *Proceedings of the 20th Intersociety Energy Conversion Engineering Conference*, Warrendale, Pennsylvania, USA, 1985.

[33] Liu Xing, Liu Hongyan, Wang Shujun, Zhang Lu, Cheng Hua, "Preparation and thermal properties of form stable paraffin phase change material encapsulation," *Solar Energy*, 80, pp. 1561-1567, 2006.

[34] Microcek Laboratories, Inc., URL: http://www.microteklabs.com/, Accessed on 03/23/2011.

[35] BASF, URL: http://www.BASF.com, Access on 03/23/2011.

[36] Hawes D.W., Feldman D, Banu.D, "Latent heat storage in building materials," *Energy and Buildings*, 20, pp. 77-86, 1993.

[37] Ruth Kelley, *Latent heat storage in building materials*, AMIAC Report.

[38] Gabbott P., *Principles and applications of thermal analysis*, Blackwell Publishing, Oxford, UK, 2008.

[39] Z.Yinping, J.Yi, J.Yi, “A Simple method, the T history method, of determining the heat of fusion, specific heat and thermal conductivity of phase change materials,” *Measurement Science Technology*, 10, pp. 201-205, 1999.

[40] ASTM Standard: “Standard Test method for steady state thermal transmission properties by means of the heat flow apparatus,” ASTM-C-518-04.

[41] URL, http://www.simulia.com/, Accessed on 08/13/2010.

[42] Design Builder, URL, http://www.designbuilder.co.uk/, Accessed on 03/23/2011.

[43] Energy Plus, URL, http://apps1.eere.energy.gov/buildings/energyplus/, Accessed on 03/23/2011.